U. S. ARMY
TRANSPORTATION RESEARCH COMMAND
FORT EUSTIS, VIRGINIA

TRECOM TECHNICAL REPORT 64-41

THE MARVEL PROJECT

AN INVESTIGATION OF THE SHROUDED PROPELLER PROPULSIVE SYSTEM ON THE MARVELETTE AIRCRAFT

Task 1D121401A14203
Contract DA 44-177-AMC-892(T)

August 1964

prepared by:

MISSISSIPPI STATE UNIVERSITY
The Aerophysics Department
State College, Mississippi

DISCLAIMER NOTICE

When Government drawings, specifications, or other data are used ofr any purpose other than in connection with a definitely related Government procurement operation, the United States Government thereby incurs no responsibility nor any obligation whatsoever; and the fact that the Government may have formulated, furnished, or in any way supplied the said drawings, specifications, or other data is not to be regarded by implication or otherwise as in any manner licensing the holder or any other person or corporation, or conveying any rights or permission, to manufacture, use, or sell any patented invention that may in any way be related thereto.

DDC AVAILABILITY NOTICE

Qualified requesters may obtain copies of this report from

Defense Documentation Center
Cameron Station
Alexandria, Virginia 22314

This report has been released to the Office of Technical Services, U. S. Department of Commerce, Washington 25, D. C., for sale to the general public.

The findings and recommendations contained in this report are those of the contractor and do not necessarily reflect the views of the U. S. Army Mobility Command, the U. S. Army Materiel Command, or the Department of the Army.

HEADQUARTERS
U S ARMY TRANSPORTATION RESEARCH COMMAND
FORT EUSTIS VIRGINIA 23604

This report is the third of a series devoted specifically to tests with the boundary-layer-control (BLC) test-bed vehicle, the Marvelette (XAZ-1). Basically, this vehicle represents the accumulation of aerodynamic design data and techniques that have been developed at Mississippi State University for the purpose of improving low-speed flight characteristics. The test information will be applied toward design refinement of the BLC research aircraft Marvel and toward the redefinition of low-speed aerodynamic research.

This report presents an investigation of the shrouded propeller propulsive system on the Marvelette aircraft and is published for the dissemination of information and the stimulation of ideas.

GARY N. SMITH
Project Engineer

PAUL J. CARPENTER
Group Leader
Applied Aeronautical
Engineering Group

APPROVED.

FOR THE COMMANDER:

LARRY M. HEWIN
Technical Director

Task 1D121401A14203
Contract DA 44-177-AMC-892(T)
TRECOM Technical Report 64-41
August 1964

THE MARVEL PROJECT

PART C

AN INVESTIGATION OF THE SHROUDED PROPELLER PROPULSIVE SYSTEM ON THE MARVELETTE AIRCRAFT

Aerophysics Research Report No. 48

Prepared by
Sean C. Roberts
The Aerophysics Department
Mississippi State University
State College, Mississippi

for
U. S. ARMY TRANSPORTATION RESEARCH COMMAND
FORT EUSTIS, VIRGINIA

CONTENTS

LIST OF FIGURES

LIST OF SYMBOLS

S Cross-sectional Area

θ Diffuser Angle

ϕ Inflow Angle to the Propeller Blade Element

T Thrust

ρ Density

U Velocity

δ Velocity Increment = $\delta_0 + \delta_1$

δ_0 Velocity Increment Due to Shroud

δ_1 Velocity Increment Due to Propeller

C_T Propeller Loading Coefficient = $\frac{T_P}{q \cdot S_{PROP}}$

q Dynamic Head = $\frac{1}{2} \rho U_{\infty}^2$

$\bar{C}_T$ Total Loading Coefficient on Shroud-Propeller Combination = $\frac{\bar{T}}{q \cdot S_{PROP}}$

$\bar{T}$ Total Thrust of Shrouded Propeller

η_i Froude Efficiency for an Ideal Propeller

P Power

λ_P Advance Ratio of Propeller

r Blade Radius

C Equivalent Blade Chord

Q Torque

C_L Lift Coefficient

C_D Drag Coefficient

T_0 Static Thrust

C_{D_i} Induced Drag Coefficient

A Aspect Ratio

e Efficiency Factor

U_R Resultant Velocity = $\sqrt{(TV)^2 + (U_\infty)^2}$

TV Tangential Velocity

U_j Jet Velocity

U_∞ Free-stream Velocity

ω Angular Velocity, Radians per Second

INTRODUCTION

The two main reasons that shrouds or ducts are placed around propellers are either: (a) for thrust augmentation or (b) for increasing the limiting Mach number of a propeller blade. Thrust augmentation has been used successfully for a number of years in the form of the Kort nozzle to increase the static thrust of tug boats; however, it has been only recently that shrouded propellers have been used on aircraft to help the acceleration and takeoff performance of STOL aircraft. The inherent circulation of the airfoil section of the shroud induces a velocity increment at the propeller plane. This increase in circulation induced by the thrust of the propeller, promotes a low-pressure region close to the leading edge of the shroud which, when integrated circumferentially, gives a resultant thrust perpendicular to the plane of the shroud. This thrust increment together with the increased efficiency of the propeller blades, due to the end-plating effect by the shroud, gives a considerable increase in thrust over the open propeller, especially in the static case or when the forward velocity is small.

The Mach number limitation of a propeller can also be increased by a shroud whose circulation decreases the inflow velocity at the propeller, thereby increasing the Mach number at which this propeller could operate efficiently. This particular use of a shroud is seldom employed and is usually only of academic interest; however, this application of a shrouded propeller should not be forgotten.

Thrust augmentation is the principal reason that propellers are shrouded, and it is the object of this report to develop a reasonably accurate method of designing a shrouded propeller for thrust augmentation. The full-scale flight experimental results of a shrouded propeller on a pusher-type aircraft will be presented and compared with the equivalent free-propeller and theoretical results developed from existing theories.

The results of this report could be used either to predict the performance of a ducted-propeller configuration or, knowing the performance required, to design the ducted propeller.

SUMMARY OF THEORETICAL METHODS USED IN THE DESIGN OF DUCTED PROPELLERS

The general problem is to determine the flow field around a ring airfoil of known camber and thickness distribution inside of which exists a pressure discontinuity normal to the axis of symmetry in the presence of a uniform free stream of arbitrary direction and magnitude. From the details of the flow field, the aerodynamic forces, moments, and overall efficiency could be calculated by integrating pressures over the various surfaces. Some of the methods of solving the above problem are briefly outlined below.

A. Method of Singularities

If this method is used, the shroud airfoil camber line is replaced by a distribution of vortices which produce the desired circulation equal to that of the shroud. Also, the effect of duct profile thickness and of centerbodies could be included by the use of additional distributed singularities. The mathematical expressions for determining the velocities induced throughout an inviscid, ideal, incompressible fluid due to an arbitrary distribution of potential vortices are well known (Reference 12) and can be used in solving for the flow field. Helmbold (Reference 5) assumed the mathematical form of the shroud vorticity distribution with unspecified coefficients for each term and satisfied the boundary condition at a number of points on the shroud equal to the number of unknown coefficients. Using this approach, Helmbold calculated the performance of a family of shrouds having assumed parabolic camber lines. These solutions of assumed vorticity distributions represent rather special cases and are not generally applicable unless a small chord-diameter ratio is assumed (Reference 17).

The mathematical difficulties encountered in the method of singularities make it very unpopular with designers who use either the momentum methods or some modified method of their own.

B. Momentum Methods

The total thrust and power relationships of a ducted propeller are quickly found by the application of Newton's second law to axial flow in front of and behind the duct. For example, the thrust can be expressed as a product of the mass flow per unit time through the duct and t change in velocity from infinity ahead to infinity behind the duct. This method is simple; however, certain assumptions must be made. The flow must be irrotational either by counterrotating propellers or

by straightening vanes. Also, it generally is assumed that the jet area at infinity downstream equals the exit area of the duct. This overcomes the necessity of resorting to the method of singularities of linking the wake area and the wake velocity with the shroud design. However, assuming that the duct exit area is equal to the wake area implies that the velocity distribution in the wake is constant and also that the static pressure at the shroud exit is equal to ambient pressure. In other words, using this theory, the entire character of the wake is assumed.

Another wake area assumption suggested by Weinig (Reference 30) and developed by Trefftz (Reference 25) is that the final wake area is related to the cross-sectional area and diffuser angle at the trailing edge of the duct; i.e.,

$$\frac{S_{FINAL}}{S_{EXIT}} = \frac{1}{1 - C_{\theta}} \qquad (1)$$

where θ is the angle of inclination of the inside surface of the duct trailing edge with respect to the duct axis. The above equation, of course, is restricted to small values of θ unless some means of boundary-layer control is applied to prevent flow separation.

C. Other Methods

These methods are generally approximate methods which either place emphasis on the propeller, by using a blade element theory and modifying the blade element theory to take some account of the influence of the shroud, or place emphasis on the shroud, which usually consists of an approximation to the method of singularities. For example, the shroud may be represented approximately by a single vortex ring (Reference 2).

An electrical analogue to the method of singularities for three-dimensional potential-flow problems has been applied to the ducted propeller problem by Malavard (Reference 14). The boundary conditions are satisfied by the application of appropriate electrical potentials at the shroud and at the wake boundary which is assumed to be of constant diameter.

In summary, it can be said that the mathematics are at our disposal for solving the problem of ducted propellers, provided that either the

shroud camber line or the shroud vorticity distribution is specified. However, the mathematics are involved and complicated, and in practical applications where the inflow to the ducted propeller is not uniform (i.e., a ducted propeller at the rear of a fuselage), approximate methods using the momentum theory developed by Kuchmann and Weber (Reference 11) are generally sufficiently accurate. Once the shroud shape is determined and the velocity distribution through the disc is calculated, the required propeller twist can be determined by using existing propeller design techniques (References 26 and 16).

THEORETICAL ANALYSIS OF THE MARVELETTE SHROUDED PROPELLER

As a propulsion system is generally an integral part of a vehicle, there are generally certain specifications with respect to size, weight, and position on the vehicle which must govern the design of the propulsion system. In the case of an aircraft with a ducted propeller, these criteria dictate that the shroud be located aft of the center-of-gravity position of the aircraft for stability reasons; otherwise, a tremendous fin area would be required to overcome the adverse yaw effect of the shroud.

On the MARVELETTE aircraft, the airfoil section of the shroud was chosen so that it had low drag at very low angles of attack, as this attitude would correspond to the cruise attitude of the aircraft. The low-drag Eppler airfoil section was modified so that the camber was increased to 4 percent and the leading-edge radius was increased to suppress possible leading-edge separation at moderate angles of attack and low advance ratios. The shroud diffusion angle is approximately 5.3 degrees, which is small enough to prevent possible diffuser separation problems.

The three-bladed MARVELETTE propeller was of variable pitch with blades of constant chord, and in the original configuration the blades were untwisted. This allowed twist modification to be easily incorporated from inflow measurements on ground running and flight tests for optimum propeller performance.

The shroud component of a shrouded propeller unit controls, to a large extent, the flow conditions at the propeller plane. Therefore, a knowledge of the annulus velocity at the propeller plane is essential to design an efficient propeller for operating within a shroud for both static conditions and at finite forward velocities.

A. Static Conditions

Newton's second law of motion gives

$$T = \rho S_{EXIT} U_j^2 \quad \text{WHERE } U_j = \text{JET VELOCITY}$$

$$\therefore U_j = \sqrt{\frac{T}{\rho S_{EXIT}}} \,, \qquad (2)$$

and from the equation of continuity for incompressible, inviscid fluid

$$U = \frac{S'_{EXIT}}{S'_{ANNULUS}} \qquad U_j = \sqrt{\frac{T S'_{EXIT}}{(S'_{ANNULUS})^2 \rho}} \quad . \tag{3}$$

For the MARVELETTE shroud

$$S'_{exit} = 28.3 \text{ feet}^2$$

T = 605 pounds anticipated thrust obtained from the universal propulser chart (Figure 5)

$$S'_{annulus} = S'_{propeller} - S'_{hub}$$

$$= 23.8 - .788$$

$$= 23.01 \text{ feet}^2$$

and the average annulus velocity in the static condition is U = 165 feet per second.

If the modification to the above theory suggested by Weinig (Reference 30), which is that the final area of the wake is not the exit area of the duct, and if the ratio $\frac{S'_{FINAL}}{S'_{EXIT}} = \frac{1}{1.04^2}$ is applied, the above results are modified to the following:

$$S'_{final} = 29.5 \text{ feet}^2$$

and U = 168.4.

A very small modification to the simple momentum theorem results.

B. Forward-Flight Conditions

At forward-flight speeds, the shroud circulation either increases or decreases the annulus velocity relative to the free-stream velocit , depending on shroud geometry. According to Kuchmann and Weber (Reference 11), this circulation has two components which are: (a) that due to inherent circulation of the shroud airfoil profile and (b) that induced by the thrust of the propeller within the shroud. The mean velocity in the annulus is

$$V = V_\infty \left(1 + \frac{V_j}{2V_\infty} + \delta\right) \tag{4}$$

where δ is the ratio of the velocity increment induced by shroud circulation to the free-stream velocity.

Also $$\delta = \delta_0 + \delta_1 \tag{5}$$

where δ_0 is that velocity increment induced by inherent circulation of the shroud and is a function of airfoil-thickness ratio and airfoil-camber ratio. Helmbold (Reference 5) correlated this information, and it is presented in Figure 6 where inherent circulation is plotted against camber ratio at various thickness ratios. From this curve it can be seen that δ_c for the MARVELETTE airfoil is 0.18.

δ_1 is the velocity increment induced by the thrust of the propeller within the shroud and can be related to the propeller thrust coefficient using potential flow methods so that

$$\delta_1 = K\left(\sqrt{1 + C_{T_P}} - 1\right) \tag{6}$$

where K is a constant of proportionality. Tests by Kuchmann and Weber (Reference 11) indicate that K varies with radial blade station and axial propeller location relative to the shroud chord. From the result of these tests in Reference 11, the value of this constant for the MARVELETTE is K = 0.4. Also from Reference 11,

$$\frac{V_j}{V_\infty} = \sqrt{1 + C_T} - 1 \tag{7}$$

where C_T = propeller loading coefficient = $\dfrac{T_P}{q \cdot S_{PROP}}$.

Also $$q = \tfrac{1}{2} \rho V_\infty^2$$

$$\bar{C}_T = C_T + \Delta \bar{C}_T$$

$$= \frac{\bar{T}}{q \cdot S_{PROP}} = \text{total loading coefficient on shroud-propeller combination}$$

and $\Delta \bar{C}_T = \kappa\delta\left(\sqrt{1 + C_T} - 1\right)$ = shroud loading.

The Foude efficiency for an ideal propeller = η_i

$$\text{where } \eta_i = \frac{\bar{T} U_\infty}{P_A} = \frac{1}{1 + \frac{U_j}{2U_\infty}} = \frac{2}{1 + \sqrt{1 + C_T}} \tag{8}$$

where P_A = power available.

To account for profile drag of the propeller, etc., in this analysis it was assumed that $\eta_P = 0.90\, \eta_i$, which is 10 percent loss in ideal efficiency. From the above relationships, it can be seen that

$$\frac{U_{ANNULUS}}{U_\infty} = 1 + \frac{1}{2}\frac{U_j}{U_\infty} + \delta = 1 + \frac{1}{2}\left[\sqrt{1 + C_T} - 1\right] + \delta$$

$$= 1 + \frac{1}{2}\left[\sqrt{1 + C_T} - 1\right] + \frac{1}{2}\left[\sqrt{1 + C_{T_P}} - 1\right] + \delta_0$$

$$= (1 + \delta_0) + 0.9\left(\sqrt{1 + C_T} - 1\right) \tag{9}$$

for the MARVELETTE shrouded propeller. From the power relationships

$$P = \frac{T U_\infty}{550} \quad \therefore \quad T = \frac{550\, P}{U_\infty} \tag{10}$$

$$\text{AND} \quad C_T = \frac{550\, P}{\frac{1}{2} U_\infty \rho_{SEA} A_P} \tag{11}$$

Therefore, power from the propeller = P_P

$$\text{where } P_P = P_A \eta_P = 0.90 \frac{2}{1 + \sqrt{1 + C_T}} P_A \tag{12}$$

Using equations 9, 10, 11, and 12, it is possible by an interative procedure to determine propulsive efficiency, thrust of shroud. and propeller unit separately and also the ratio of the annulus velocity to the free-stream velocity.

Example: The MARVELETTE shroud - 83 horsepower available, which is 90 horsepower developed from the C90 engine minus the 7 horsepower required to operate the blowers for the high-lift boundary-layer control system for the aircraft.

S prop = 23.01 feet^2, S exit = 28.3 feet^2, chord = 2.67 feet,
Climb-out, full throttle, U_∞ = 80 feet per second, q = 7.6.

First Approximation -

$$\eta_p = .50, \quad P_A = 85 \text{ horsepower}$$

$$P_p = \eta_p P_A = 41.5 \text{ horsepower}$$

$$T_p = \frac{550 P_p}{U_\infty} = 285 \text{ pounds}$$

$$C_p = \frac{T_p}{q S_{PROP}} = 1.58$$

and $$\eta_p = (0.90)\frac{2}{1+\sqrt{1+C_T}} = .69$$

Second Approximation -

$$\eta_p = .69, \quad P_p = 57.3 \text{ horsepower}$$

$$T = 394 \text{ pounds}$$

$$C_T = 2.17$$

$$\eta_p = .648$$

Third Approximation -

$$\eta_p = .648, \quad P_p = 53.8$$

$$T = 370 \text{ pounds}$$

$$C_T = 2.04$$

$$\eta_p = .654$$

$$\delta_1 = .4(\sqrt{1+C_{T_p}} - 1) = .296$$

Thrust on the Shroud -

$$\Delta \bar{c}_T = 2\delta(\sqrt{1+C_T} - 1)$$ which is the shroud loading

$$= 2(\delta_0 + \delta_1)(\sqrt{1+C_T} - 1)$$ where δ_0 = .18 for the MARVELETTE shroud airfoil section

$$\Delta \bar{c}_T = 2\ (.376)(.74)$$

$$\Delta \bar{c}_T = .556$$

$$\Delta \bar{T} = \Delta \bar{c}_1 q S_{PROP} = (.556)(7.6)(23.01)$$

= 97.5 pounds

$\bar{T}$ = 97.5 pounds + 370 pounds

= 467.5 pounds

= total thrust from shroud-propeller combination which neglects the drag of the shroud.

Velocity Through Propeller -

$$\frac{U_{ANNULUS}}{U_\infty} = (1 - \delta_o) + 0.9\left(\sqrt{1+C_T} - 1\right)$$

$$= 1.18 + .667$$

$$= 1.847$$

$\therefore$ $U_{annulus}$ = 147.6 feet per second U_∞ of 80 feet per second

Advance Ratio -

$$\lambda_p = \frac{U_{ANNULUS}}{\omega R}$$

$$= \frac{147.6}{(262)(2.75)}$$

$$= .204$$

where ω = angular velocity in radians per second and R = radius of propeller blade = 2.75 feet

$\omega = \left(\frac{RPM}{60}\right) 2\pi$ radians per second = 262 radians per second for r.p.m. = 2500

The above calculations were repeated for forward-flight velocities ranging from 40 feet per second to 360 feet per second and are tabulated below.

U_∞	$\Delta\bar{T}$	$-D$	$\bar{T} = TP + \Delta\bar{T}$	$\frac{U_{ANNULUS}}{U_\infty}$	λ_p
40	103.24813	469.79556	572.04369	3.31546	.18405
80	173.86421	373.51401	547.37822	1.85495	.20596
100	209.24569	332.10375	541.34944	1.60683	.22302
120	249.0138	295.93391	544.94771	1.46245	.24357
150	321.36086	251.18301	572.54387	1.34279	.27955
200	483.19510	197.18746	680.38256	1.25522	.34843
250	699.66709	160.76542	860.43251	1.220032	.42332
300	970.23327	135.18090	1105.41417	1.20355	.50113

It can be seen from the above tabular results of $\bar{F}$ that the thrust initially decreases with forward velocity, and then it increases again. This increase is due primarily to the influence of the value of the inherent circulation, ζ_0 , at high speeds where it is of a larger order of magnitude than ζ_1 , the circulation due to the action of the propeller. It could be possible that the value of the inherent circulation changes with forward velocity due to the flow entering the shroud more axially as the ratio of the circulation velocity to the free-stream velocity becomes smaller as the forward velocity increases. In view of this, the above propeller calculations were repeated with $\zeta_0 = 0$. This value was chosen because of a lack of information on the subject, and it has been suggested by Kuchmann and Weber (Reference 11) that for shrouds of small chord-to-diameter ratios, the velocity increment due to the shroud alone is small and can be neglected. The MARVELETTE, with a chord-to-diameter ratio of 1:4.3, could be considered in this category, and the propeller calculations with $\zeta_0 = 0$ are tabulated below.

V_∞	$\Delta \bar{F}$	$\bar{F}$	$V_{ANNULUS}/V_\infty$	λ_0
40	203.91126	673.70682	3.13546	.17407
80	81.22333	454.73734	1.67495	.18598
100	50.72949	382.83324	1.42683	.19803
120	32.22599	328.15990	1.28245	.21359
150	16.58062	267.76363	1.16279	.24208
200	6.22587	203.41333	1.07522	.29846
250	2.82994	163.59536	1.04003	.36087
300	1.32441	136.50331	1.02355	.42618

Curves of thrust and velocity ratios for both values of inherent circulation are plotted in Figures 7 and 8.

APPROXIMATE METHOD OF SHROUDED-PROPELLER DESIGN

Due to the fact that shrouded propellers usually operate on the rear of the vehicles where the inflow velocity consists of a combination of free-stream velocity and body-wake velocity, it is difficult to design an optimum shrouded propeller without knowing the influence of the vehicle on the inflow velocity field of the propeller. Therefore, an approximate design method is usually sufficiently accurate to build the shrouded propeller, and the twisting of the propeller blade can be left until after ground testing and acceleration runs are made to optimize the propeller for the particular inflow velocity conditions.

The following is a brief step-by-step outline of a method that can be utilized in the design of shrouded propellers:

1. If the horsepower available and the approximate diameter of the shroud (which would be determined from vehicular specifications) are known, the static thrust can be obtained from Figure 5. The average annulus velocity can be calculated from equation 3 in the previous section.

2. The propeller rotational velocity can be determined from the characteristics of the power source.

3. Select a shroud airfoil section according to the utilization and speed of the vehicle; i.e., select large camber and thickness ratios to give large values of inherent circulation for static and very low-speed cases and small camber and thickness ratios for high-speed cases. It should be noted that the leading-edge radius of the airfoil section chosen should be increased slightly to reduce the possibility of leading-edge separation. Also, the diffusion angle of the shroud should not exceed 7 degrees without boundary-layer control to prevent possible turbulent-boundary-layer separation.

4. Select a propeller airfoil section which gives a high lift-to-drag ratio when operating at small angles of attack and at low Reynolds numbers. Although it would be better for the propeller chord to increase toward the tips (Reference 11), for simplicity of structural design and for propeller versatility, the chord could remain constant.

5. If the theory developed in the previous section is used, values of the shroud-propeller thrust together with the average annulus inflow velocity can be calculated. It must be noted that this theory assumes a constant annulus inflow velocity. This is not normally the case, which is another point in favor of twisting the propeller according to experimental results rather than some theoretical method.

6. If the equivalent blade chord is constant with radius and if it is assumed that the blade is twisted such that each blade element is operating at a lift coefficient close to the value chosen, then the torque of each blade element can be calculated and integrated over the blade radius to give total torque. The torque equation used can be developed from the blade element diagram shown in Figure 9:

$$\frac{1}{c}\frac{dQ}{dr} = r(C_L \sin\phi + C_D \cos\phi)\tfrac{1}{2}\rho V_R^2$$

where c is the equivalent chord of the propeller

and $\phi = \tan^{-1}\frac{V_{ANNULUS}}{\text{TANGENTIAL VELOCITY}}$

r = blade radius

$$\int_{ROOT}^{TIP}\frac{1}{c}\frac{dQ}{dr} = \frac{\text{Horsepower available (obtained from engine specifications)}}{\text{Angular velocity of the propeller in radians per second}}.$$

The above integral can be performed graphically, and from this equation the value of c can be determined, which can be divided into the number of blades required on the propeller. The maximum solidity of the propeller should be limited to 0.8 since experimental data show that the aerodynamic characteristics of airfoils decrease quite rapidly when tested in cascade at solidities above 0.8.

7. The thrust developed by the propeller can be found from the equation in the previous section which assume a 10 percent decrease for propeller losses; however, the propeller thrust can also be calculated from the following equation, which is developed from Figure 9, assuming that the propeller is operating at small angles of attack:

$$\frac{dT}{dr} = (C_L \cos\phi - C_D \sin\phi)\tfrac{1}{2}\rho V_R^2 c .$$

The total propeller thrust would be equal to $\int_{ROOT}^{TIP}\frac{dT}{dr}\,dr$.

8. A plot of ϕ against r would be the approximate twist distribution for the propeller blade. This would be a first approximation, and it would be modified by experimental results at a later date. A straight, untwisted blade performs adequately in a shroud and could also be used as a first approximation to the twist distribution.

9. The falloff in thrust with forward velocity can be calculated using the method detailed in the previous section.

10. The effect of changing r.p.m. and engine power settings can be investigated in a manner similar to that described above, and it will be found that the percentage change in advance ratio with change in forward

velocity is smaller for a ducted propeller than for a free propeller. The change in advance ratio may be small enough for the operating range of the aircraft such that a fixed-pitch propeller could be used instead of a variable-pitch propeller.

The above approximate method of design assumed nonrotational flow leaving the shrouded propeller; however, even though the assumptions are considerable, the method seems to perform satisfactorily.

DESCRIPTION OF TEST EQUIPMENT AND EXPERIMENTAL PROCEDURES

A. Shrouded and Unshrouded Propellers

The shrouded propeller used in the tests was the propulsion system of the MARVELETTE aircraft shown in Figure 1. Detailed drawings and photographs of the shroud are shown in Figures 2 and 3 and the propeller used in the shroud is drawn in Figure 4. During the initial testing phase, the blade was untwisted; however, due to variations in blade thickness, the effective aerodynamic twist was found by an examination of the blade section at various stations and the results are plotted in Figure 4. The shroud also incorporated the longitudinal and directional flying controls which are generally used on aircraft. These control surfaces were constructed so that very little gap existed at the trailing edge of the shroud, irrespective of control surface position. The propeller diameter was 5 feet 6 inches, and the propeller pitch was controllable within the range shown in Figure 23. Unfortunately, due to a lack of extra slip rings on the propeller shaft, a propeller-pitch-position indicator was not available. The propeller was driven by a 5-foot fiberglass shaft attached to a Continental C-90 engine which developed 90 horsepower at 2500 r.p.m.

The unshrouded-propeller propulsion system used in the tests was that of the Anderson and Greenwood AG-14 aircraft, which is a two-place pusher aircraft with a 6-foot diameter constant-pitch propeller also powered by a C-90 Continental engine (Figure 10).

B. Static Thrust Measurements

The static thrust generated by the shrouded propeller of the MARVELETTE was found from tethered tests. The aircraft was positioned in the hanger with the tail facing through the open doors, and a cable was attached to the skid which protected the shroud from contact with the ground. Close to the ground attachment point, which was approximately 15 yards behind the propeller, a direct-reading spring balance was incorporated in the line. Care was taken to insure that the aircraft was on level ground and that the angle of the tethering cable to the ground was not very different from the angle of the thrust line to the ground. Although the tests were performed early in the morning when the wind was generally calm, the aircraft was inside the hanger to eliminate any crosswinds which could possibly promote flow separation in the shroud in the static condition.

The thrust was read directly from the spring balance at various engine r.p.m.'s and manifold pressures and is plotted in Figure 11. Readings were also taken with the moveable control surfaces in various positions, but it was found that control positions had little or no effect on static thrust.

The above test was repeated for the Anderson and Greenwood aircraft, and the full throttle results are plotted in Figure 11.

C. Dynamic Thrust Measurements

Thrust measurements at a finite forward velocity were obtained in a manner similar to the static thrust measurements except that instead of the retaining cable being fixed in the ground, it was attached to a ground vehicle. The aircraft towed the ground vehicle along, using the cable with the spring balance attached, which could be read directly from the jeep, the ground vehicle used in these tests. Full throttle was used in the aircraft, and the forward velocity was regulated in the jeep by the use of brakes. The observer in the jeep read the pull of the aircraft when steady static conditions were established. A number of tests were performed at speeds up to 40 m.p.h. in opposite directions on the main runway to eliminate both ground slope and wind effects, and the average thrust obtained in this manner is plotted in Figure 12. Due to the relatively short runway, 5000 feet, and the difficulty in establishing steady static conditions, forward speeds above 40 m.p.h. were not attempted using this direct measuring system.

To obtain experimental values of rolling friction, the aircraft was towed behind the jeep at speeds up to 40 m.p.h., and values of the rolling friction drag were read directly from the spring balance. The tests were repeated on opposite directions on the main runway, and the results are plotted in Figure 13.

D. Flow Visualization Tests

As it was necessary to find whether any serious separation or irregularities occurred in the flow around the shrouded propeller, a considerable number of flow visualization studies were performed using tuft and sublimation techniques. Small black wool tufts were stuck to the inside of the shroud, forward of the propeller plane, to indicate possible flow separations prior to entering the plane of the propeller. String was stretched across the shroud, both fore and aft of the propeller, and tufts were tied to the string at regular intervals as shown in Figure 14. Photographs were taken of these tufts from various angles while the engine was running with the propeller in fine pitch, which

would be the condition prior to takeoff. Tuft photographs were taken only in the static condition.

The sublimation technique consists of spraying a saturated solution of napthalene in petroleum ether onto the test surface. The napthalene is removed from the regions of high shear by the action of the boundary layer or attached vortices, and in regions of low shear or where the flow is separated, the white deposited napthalene will remain on the surface. In the static condition, the shroud and the propeller were sprayed and photographs were taken every few seconds of both the shroud and the propeller with the engine operating at full throttle. To obtain sublimation photographs in the dynamic case where the aircraft had a forward velocity, photographs of both the shroud and the propeller were taken at the end of each acceleration run on the runway where the aircraft was accelerated to 60 m.p.h. The aircraft was then stopped as quickly as possible with the engine off. These acceleration runs were repeated, and successive sublimation photographs of the flow about the shroud and propeller were obtained and can be seen in Figure 15.

E. Propeller Inflow Measurements

To measure the magnitude of the velocity of the air into the plane of the propeller, a static pressure rake was constructed as shown in Figure 16. The rake extended from the fuselage to the shroud and could be moved to different angular positions in the shroud. Static orifices were drilled on both sides of the symmetrical rake, the orifices on opposite sides of the rake at the same radius were connected, and a tube which gave the mean pressure on either side of the rake was connected to a photomanometer.

The photomanometer (Figure 17) had 52 'U' tubes, with 26 of them connected to a common pressure source, which in this case was the aircraft static pressure source from the nose probe. The camera was in the plane of the banks of manometer tubes, and the camera photographed the reflection of the manometer tubes in a front-surfaced mirror. This enabled the length of the manometer to be reduced approximately 50 percent. Also recorded by the manometer camera was an inclinometer which gave the correction angle if the aircraft was in a position other than level during recording. A clock and a five-light binary identification system were also recorded by the camera.

Inflow measurements were obtained at five positions in the shroud, shown schematically in Figure 18 at different aircraft airspeeds and camber settings. Care was taken to insure that steady static conditions prevailed before the data was recorded photographically. The inflow measurements are plotted in Figures 19 and 20.

From the inflow measurements and a knowledge of the propeller r.p.m. where the angular velocity of each blade element can be calculated, it is a comparatively simple matter to obtain the angle ϕ, which is the effective angle of the inflow to the propeller blade element (Figure 21). Curves of ϕ against propeller radius are plotted in Figures 21 and 22.

F. Acceleration Tests

At the conclusion of the dragging tests, to find the accelerating force of the propulsion system of the aircraft at various forward velocities by direct measurements, it was seen that a more refined and less hazardous method must be developed. As forces are difficult to measure, it was decided to measure aircraft displacement with respect to time from which could be obtained the aircraft velocity by $\frac{dx}{dt}$ and the acceleration by $\frac{dv}{dt}$. Knowing the aircraft weight and the acceleration, it is a simple matter to find the accelerating force using Newton's second law of motion.

An instrument was developed by the department (Figure 24) which would give an accurate and repeatable plot of aircraft displacement from a fixed point as a function of time. A clockwork mechanism, taken from a 35mm spring-wound movie camera, was used to rotate a small cylinder at a constant speed. A sheet of graph paper was placed on the cylinder. A large drum, on which was coiled 1000 feet of stretched Dacron cord, was connected by a gear system to a screwworm whose axis was parallel to the axis of the recording cylinder. A spring-loaded pen mounted on a threaded base sat on the screwworm; and when one end of the cord was carried off by the accelerating vehicle, the drum rotated and moved the recording pen logitudinally along the recording cylinder, which was rotating at a constant speed. The resulting curve was a record of displacement against time. It was, of course, necessary that this instrument be calibrated prior to use in the experiments. A small parachute was attached to the aircraft, on the end of its cord, which opened when the cord had reached its limits and thus prevented backlash.

Eight acceleration runs were performed with the MARVELETTE aircraft from both ends of the runway, and the results are plotted in Figure 25. A mean curve was chosen and was used in Figure 27, which is a thrust breakdown chart incorporating the aircraft rolling friction and the estimated aerodynamic drag of the MARVELETTE. Similarly, six acceleration runs were performed on the AG-14, and the results are plotted in Figure 29. The mean curve was taken and used in the thrust breakdown chart in Figure 30.

G. Flight Instrumentation

The aircraft was well instrumented, and visual representation of all the control surface movements was available on the cockpit panel together with all pertinent aircraft instruments and blower instrumentation. The complete instrument panel was photographed every 2 seconds by a 16mm movie camera located in the rear of the cabin. The pictures from this movie camera were correlated with the pictures taken in the photomanometer by the simple means of placing synchronized clocks in the instrument panel and in the manometer. When this technique was used, all pertinent aircraft flight data were available for every frame taken of the manometer.

DISCUSSION OF RESULTS

The theoretical techniques described in the third and fourth sections of this report represent a very simple and effective method of either designing or predicting the performance of a ducted propeller. This method was developed from momentum considerations used by Kuchmann and Weber (Reference 11); however, great care should be used in applying the inherent circulation correction developed by Helmbold (Reference 5), especially in the case of the shrouded propeller at a finite forward velocity. As can be seen from Figure 7, for shrouds of relatively large diameter-to-chord ratio, the most representative thrust-versus-forward-velocity curve of experimental results is that where the inherent circulation, ζ_0 , was taken to be zero. What the critical shroud diameter-to-chord ratio is where ζ_0 must be taken into consideration, is at the present time unknown. Figure 8, which represents the variation of advance ratio and annulus velocity with forward velocity at two values of inherent circulation, shows that in the design case the effect of ζ_0 is less important than in the performance case.

The experimental static thrust results presented in Figure 11 indicate a maximum static thrust of 600 pounds from this configuration, whereas the predicted result from Figure 5 was 605 pounds. A 7-percent decrease in static thrust was tolerated in order to optimize the propeller blades for the aircraft climb-out conditions. This was done by incorporating the blade twist modifications shown in Figure 23. This modification considerably improved the climb-out characteristics of the MARVELETTE aircraft, thereby making the aircraft much safer in the initial climb-out phase of operation.

The acceleration curves obtained by towing a ground vehicle behind the aircraft and directly reading the thrust at various forward velocities leaves much to be desired and is not recommended at forward velocities greater than 30 m.p.h. The difficulty of maintaining steady conditions for any length of time and the possibility of damaging either the aircraft or the ground vehicle in any emergency is very high. The results obtained by this method are presented in Figure 12 and are compared in Figure 25 with the results obtained using the accelerometer.

The flow visualization results obtained (Figures 14 and 15) using tufts and the sublimation techniques show quite clearly that in the static condition and at low forward velocities a small laminar separation bubble exists on the leading edge of the shroud. This small bubble is probably responsible for the intermittent flow separation occurring forward of the propeller plane on the shroud, as shown in Figure 14C. The flow leaving the shroud has considerable rotation, as can be seen from Figure 14B, and the flow field around the spinner shows considerable separation from the spinner and the blade root fiberglass cuffs. The sublimation photo-

graphs of the propeller indicate that an appreciable amount of laminar flow exists on the blades. Also flow separation occurs on the fiberglass blade root cuffs, indicating that either the blade twist or the cuffs could be modified to eliminate this flow separation. From these results it can also be observed that the tip clearance between the blade and the shroud is sufficiently small to reduce or almost to eliminate the tip clearance vortex described in Reference 27.

The propeller inflow measuring rake shown in Figure 16 with the cross-connected static orifices performed satisfactorily in measuring the annulus inflow velocity to the propeller in conjunction with the multi-tube manometer (Figure 17). Figure 18 shows the results of measurements taken at five angular stations to determine how symmetrical was the flow into the shroud. The flow is very symmetrical except at the two bottom positions on either side of the fuselage, where the inflow-velocity component is smaller than at any other station in the shroud. This small variation in inflow velocity is less than 5 percent; however, this is one of the reasons that an approximate theoretical method is used to determine propeller inflow velocities because of the rather unpredictable effects of the fuselage proximity and mainplane downwash on the inflow distribution. The inflow-velocity distributions show quite clearly that in all angular positions in the shroud, the inflow velocity is not a constant as is assumed by the momentum theories. The theoretical results, for example, estimate that in the static condition the average inflow velocity is 165 feet per second, whereas it can be clearly seen in Figure 19 that the average inflow velocity is of the order of 130 feet per second and that only a small region near the tip of the blade has an inflow velocity of 161 feet per second. It is, of course, possible that only the outer region of the propeller blade is operating effectively and, as will be discussed later, this is just the case. Changes in wing camber or equivalent flap angle do not appreciably affect the inflow velocity to the propeller plane. Figure 20 shows that the axial velocity into the propeller decreases very slightly with an increase in wing camber.

Changes in aircraft airspeed have very detrimental effects on propeller blade effectiveness, as can be clearly seen in Figure 22A where the propeller blade was in the original untwisted condition. At an aircraft airspeed of 70 m.p.h., the outer 18 inches of the blade is operating with only a small radial portion at an optimum angle of attack; and at 110 m.p.h., only the outer 9 inches is operating, and the remainder of the propeller is windmilling. This is probably the reason for the nonuniform inflow-velocity distributions and is undoubtably the reason for the poor climb-out performance of the aircraft at 90 m.p.h. The propeller blade twist modifications described in Figure 23 helped to relieve this problem, as can be seen in Figure 22B from the results using the twisted blade. At 110 m.p.h., a 15-inch portion of the blade is operating at a reasonably constant angle of attack in comparison to 9 inches at a continuing varying angle of attack for the straight blade.

This modification helped the overall propeller performance; however, as can be seen in Figure 22B, further small modifications to the twist distribution of the propeller blade would increase performance.

The apparatus used in the acceleration tests of the MARVELETTE and the AG-14 aircraft gave reasonable results, as can be seen in Figure 25. These results compare reasonably well with the results of the accelerating force obtained from the dragging tests. This technique of measuring the variations of thrust with forward velocity is very effective up to speeds below the takeoff airspeed of the aircraft, and by careful piloting, the technique can be used at ground speeds in excess of the minimum flying speed of the aircraft. The thrust breakdown chart (Figure 27) shows that the propulsor thrust falls off quite rapidly with forward velocity. Any errors involved in the drag estimate of the MARVELETTE aircraft (Appendix) would be negligible on the final result of this thrust curve; however, in the extrapolation to flight speeds this would not be the case, and errors of the order of 15 percent could easily be incorporated in the results. It is very interesting to note that the estimated maximum velocity of the aircraft, using the assumed estimated aerodynamic drag and a linear variation in thrust, is remarkably close to the measured maximum velocity of the aircraft. This, of course, means that either the assumptions are relatively correct or else the errors involved are compensatory. Similar acceleration techniques applied to the open propeller on the AG-14 produced thrust curves of a similar shape to the MARVELETTE thrust curves (Figures 29 and 30).

An attempt was made to fit equations to the thrust curves, and for the open-propeller case, a linear variation according to $T = T_0 - 2.4V$ is adequate. Similarly, the equation $T = T_0 - 0.6V^{1.26}$ gives a reasonable fit to the curve up to forward velocities of 80 feet per second. For the case of the shrouded-propeller thrust curve, as can be seen in Figure 31B, a number of equations give reasonable results, the most useful on being

$$T - T_0 = 38.337 - 4.493V + .000127V^3 - .000033V^4.$$

To use this equation means that T_0 must be known, and it can be found quite accurately as demonstrated by the MARVELETTE shrouded-propeller results from Figure 5.

In an attempt to determine the shroud break-even velocity, which is that velocity where the thrust increment due to the shroud equals the drag of the shroud, Figure 32 was drawn. The theoretical break-even velocity is 152 feet per second, assuming that the ring tail is additional to the conventional tail plane; however, in the MARVELETTE case, where the conventional tail plane is eliminated, the break-even velocity is 162 feet per second. Although the experimental results agree reasonably well with the theoretical value of the shroud thrust at low forward velocities, it can be seen that at high forward velocities considerable differences occur. If the experimental curve were extrapolated

to higher velocities, the experimental break-even velocity would be greater than 200 feet per second, although the accuracy of this extrapolation would be debatable.

Finally, a comparison was made between the theoretical and experimental total thrusts obtained for the MARVELETTE shrouded propeller (Figure 34). The experimental curve is considerably lower than the theoretical curve. This is to be expected because, in the theoretical case, it was assumed that the complete propeller was operating at an optimum blade angle of attack, which, of course, was not the case, as was discussed above and is shown in Figures 21 and 22. From Figure 34, it can be seen that both curves have essentially the same shape and that the experimental curve is approximately 75 percent of the theoretical curve.

CONCLUSIONS

The theoretical methods of shrouded-propeller design and performance predictions outlined in the third and fourth sections of this report are adequate even though the results tend to be optimistic. The differences between theoretical and experimental results are due primarily to insufficient or improper blade twist, especially around the blade root. Shroud leading-edge laminar separation bubbles and flow separation around the spinner also contribute to the difference in results.

Due to the difficulty of predicting flow fields into shrouded propellers because of the presence of the fuselage and wing, etc., it is felt that the approximate momentum methods used in this report are more practical for the design of ducted propellers than the more exact and rigorous method of singularities.

The static thrust of the shrouded-propeller configuration was approximately 100 percent greater than the static thrust of the equivalent open propeller driven by the same horsepower engine.

The decrease in propulsor thrust with forward velocity has been found experimentally up to velocities of 100 feet per second, and from theoretical considerations, it was found that the break-even velocity for the MARVELETTE aircraft is 162 feet per second. However, if the experimental curve were extrapolated, break-even velocities greater than 200 feet per second could be expected. Equations for the variations of thrust for both an open and a shrouded propeller have been developed. Considerable work needs to be performed on the variation of propulsor thrust with forward velocity, especially at speeds in excess of 100 feet per second. This work could be performed either in a large wind tunnel or on high-speed ground vehicles where the thrust could be measured directly.

Using the methods described in this report, it is possible to design a shrouded propeller or to predict the performance of a shrouded propeller to within an accuracy of about 10 percent.

BIBLIOGRAPHY

1. Abbott, I. H., Von Doenhoff, A. E., and Stivers, L. S., Summary of Airfoil Data, NACA Report No. 824, Langley Field, Virginia, 1945.

2. Allen, H. J., and Rogallo, F. M., Ring-Cowled Propellers, Department of Mechanical Engineering, Stanford University, Stanford, California, 1935.

3. Fletcher, H. S., Experimental Investigation of Lift, Drag, and Pitching Moment of Annular Airfoils, NACA TN 4117, Langley Field, Virginia, October 1957.

4. Hawwa, L., Underwater Static Test on Shrouded Propellers, Aerophysics Department, Mississippi State University, State College, Mississippi, 1957.

5. Helmbold, H. B., Range of Application of Shrouded Propellers, University of Wichita Engineering Report No. 189, Wichita, Kansas, 1955.

6. Hoehne, V. O., Aerodynamic Characteristics of a Shroud with Centerbody, University of Wichita Engineering Report No. 337, Wichita, Kansas, February 1959.

7. Hoehne, V. O., A Method of Design of Shrouded Propellers, University of Wichita Engineering Report No. 213-8, Wichita, Kansas, October 1959.

8. Hoehne, V. O., and Hoffman, H., Shrouded Propeller Investigations: Propeller Tip Clearance Effects, University of Wichita Engineering Report 213-215, Wichita, Kansas, 1961.

9. Hoerner, S. F., Fluid Aerodynamic Drag, Published by the Author, Midland Park, New Jersey, 1958.

10. Jackes, A. M., Ducted Propeller Developments at Bell Aircraft, Bell Aircraft Corporation, Buffalo 5, N. Y., presented M. I. T., December 3-6, 1958, Symposium.

11. Kuchmann, D., and Weber, J., Aerodynamics of Propulsion, McGraw-Hill Book Company, New York, 1953.

12. Lamb, H., Hydrodynamics, Sixth Edition, Dover Publications, New York, 1945.

13. Lippisch, A. M., Some Basic Deviations About the Action of a Ducted Propeller, Collins Aeronautical Research Laboratory, Cedar Rapids, Iowa, 1956.

14. Malavard, L., and Jacques, G., Problems de L'Aile Annulaire Resolus per Anologie Rheoelectrique, Laboratorie de Calcul Analogique der CNRS, Paris, France, September 1958.

15. McNay, D. E., Study of the Effects of Various Propeller Configurations on the Flow About a Shroud, Research Report No. 14, Aerophysics Department, Mississippi State University, State College, Mississippi, 1958.

16. Patterson, G. N., Ducted Fans, Design for High Efficiency, Australian Council for Aeronautics, Report ACA-7, 1956, ASTIA AD 85 451.

17. Pivko, S., "The Annular Airfoil with Centerbody and Propeller", Aircraft Engineering, Vol. 29, p. 353, November 1957.

18. Platt, Jr., R. J., Static Tests of a Shrouded and Unshrouded Propeller, NACA RM L 7H25, Langley Field, Virginia, 1948.

19. Roberts, S. C., Flight Testing of the MARVEL and MARVELETTE Airfoil Sections, Report No. 38, Aerophysics Department, Mississippi State University, State College, Mississippi, 1962.

20. Sacks, A. H., and Burrell, J. A., Ducted Propellers - A Critical Review of the State of the Art, Report No. ARD-232, Advanced Research Division of Hiller Aircraft Corporation, Palo Alto, California, 1959.

21. Seibold, W., Approximate Calculations of the Shrouded Propeller, Aero. Report 904, Donald W. Taylor Model Basin, Washington 25, D. C., 1956.

22. Sinacori, J., and Lauge, A., Theoretical Investigations of Ducted Propellers, Republic Aviation Corporation, Farmingdale, Long Island, New York, September 1961.

23. Theodorsen, T., Ducted Propeller Aerodynamics, Republic Aviation Corporation, Farmingdale, Long Island, New York, 1960.

24. Thompson, J. S., et. al., Comparison of Pusher and Tractor Propellers Mounted on a Wing, ARC, R&M 2516, Aeronautical Research Council, Ministry of Supply, London, England, 1951.

25. Trefftz, E., Uber die Kontraktion kreisformiger Flussigkeitsstrahlen, Zeitschrift fur Mathematik und Physik, 1916.

26. Wallis, R. A., Design, Performance and Analysis of Ducted Axial Flow Fans, Department of Supply Research and Development Branch, ARL Australian ARL Report No. A. 88, NASA N-34375.

27. Wattson, Jr., R. K., Note on Blade Tip Effects in Shrouded Propellers, University of Wichita, Engineering Report No. 333, Wichita, Kansas.

28. Wattson, Jr., R. K., Note on the Static Performance of Shrouded Propellers, University of Wichita, Engineering Report 307, Wichita, Kansas.

29. Wood, K. D., Airplane Design, Published by the Author, Boulder, Colorado, 1954.

30. Weinig, F., Aerodynamik der Luftschraube, Springer Verlag, Berlin, 1940.

APPENDIX

Estimated Drag Breakdown of the MARVELETTE Used in the Thrust Evaluation Tests

The following estimate was obtained using References 1, 9, and 29 for component drag coefficients. It was assumed on the takeoff run with the nose wheel on the ground that the angle of attack was approximately zero, which, according to Reference 19, is equivalent to a lift coefficient of 2.3.

Component	Drag Coefficient	Area Based on	Drag at 100 ft./sec.
Wing (zero angle of attack)	$C_D = .005$	Wing Area	6.3 lb.
Fuselage	$C_D = .05$	Fuselage Cross-sectional Area	8.5 lb.
Shroud	$C_D = .01$	$(c)(2\pi\ell)$	7.25 lb.
Landing Gear	80% of Fuselage Drag		6.8 lb.
Interference Drag	15% of Parasitic Drag		4.5 lb.
		Total Drag at 100 ft./sec.	33.35 lb.

MARVELETTE wing area = 106 feet^2

MARVELETTE friction drag $[C_D]$, friction based on aircraft wing area = .0264

Induced drag coefficient throughout the takeoff run = $\frac{C_L^2}{\pi A e}$ = .0026 which will be constant until rotation at the take-off velocity.

Total aerodynamic drag coefficient = $C_{D\text{friction}} + C_{Di}$

$C_{D\text{total}} = .0264 + .0026$
$= .0290.$

Ground Velocity (feet per second)	Aerodynamic Drag During Ground Run (pounds)
10	.365
30	3.3
50	9.1
80	23.1
100	36.5

Aerodynamic Drag During Flight:

$$C_{D_{TOTAL}} = C_{D_0} + \frac{C_L^2}{\pi A_c}$$

V_∞ FT./SEC.	C_L	C_{D_i}	C_D	DRAG LB.
100	1.57	.143	.169	213.2
120	1.09	.069	.095	173.9
135	.861	.043	.0694	159.4
150	.697	.028	.055	154.8
180	.484	.0136	.040	163.5
200	.392	.0089	.0353	178.1
250	.251	.0037	.0301	236.8
280	.2001	.0023	.0287	283.8

Figure 1. MARVELETTE Aircraft With Shrouded Propeller.

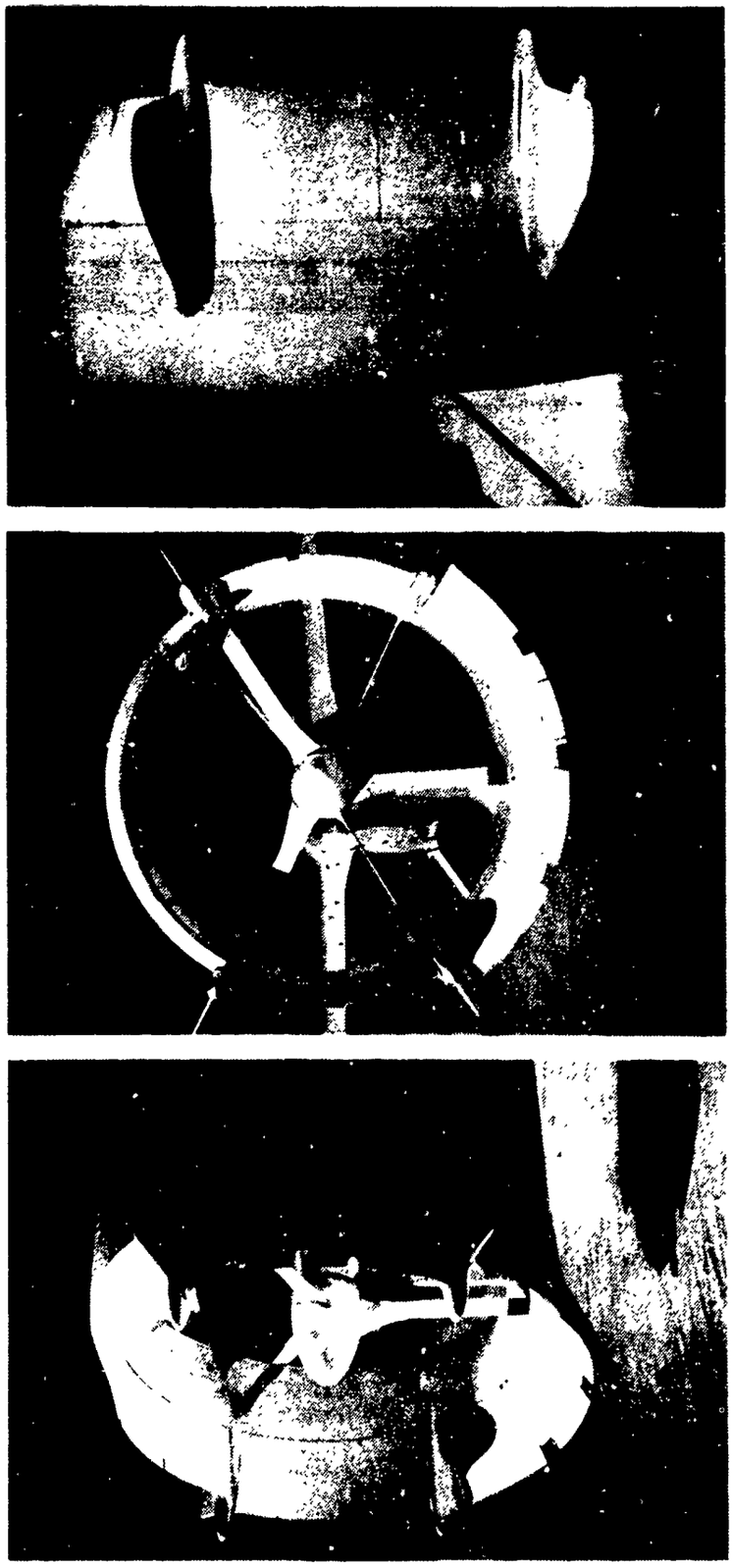

Figure 2. Three Views of the Shrouded Propeller.

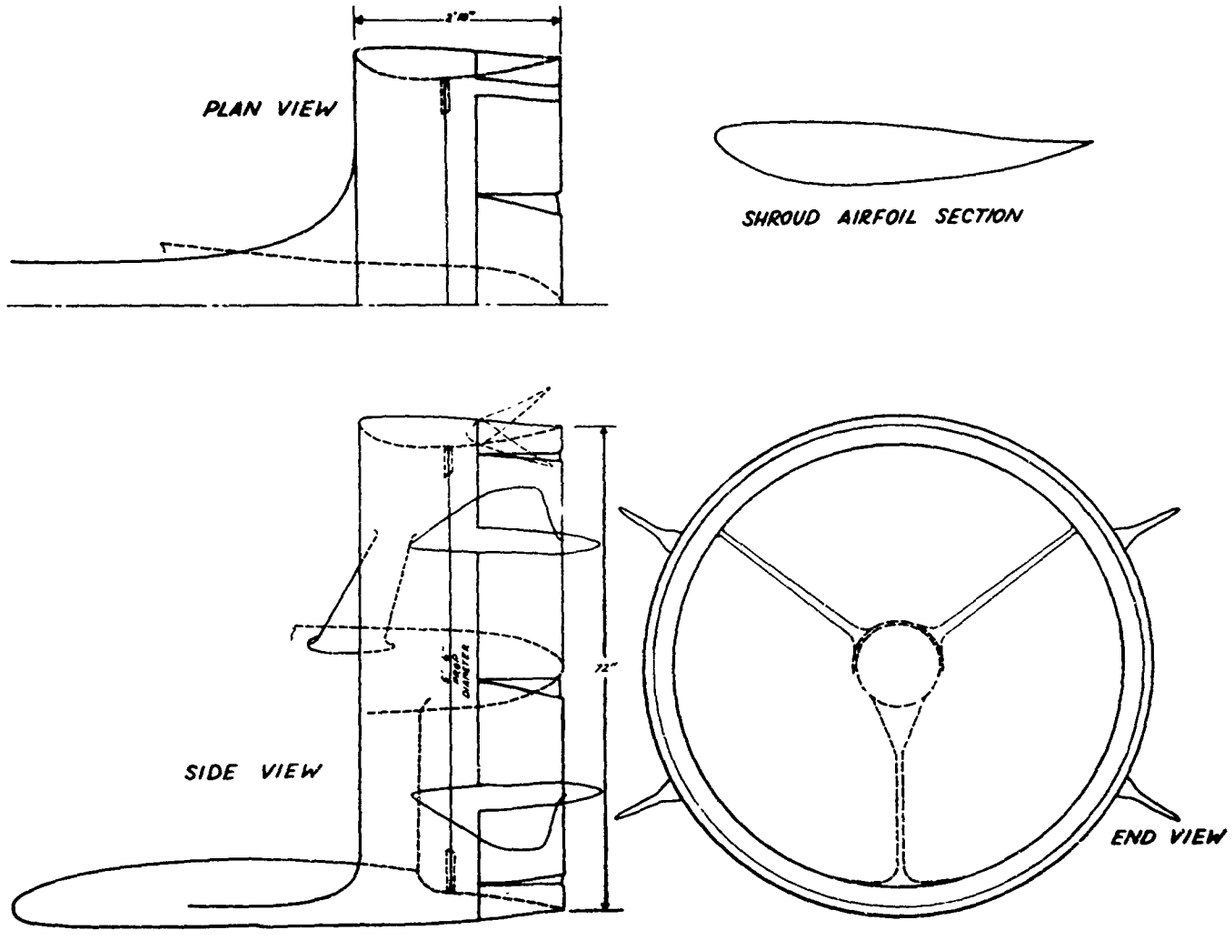

Figure 3. Detailed Geometrical Drawing of the Shroud.

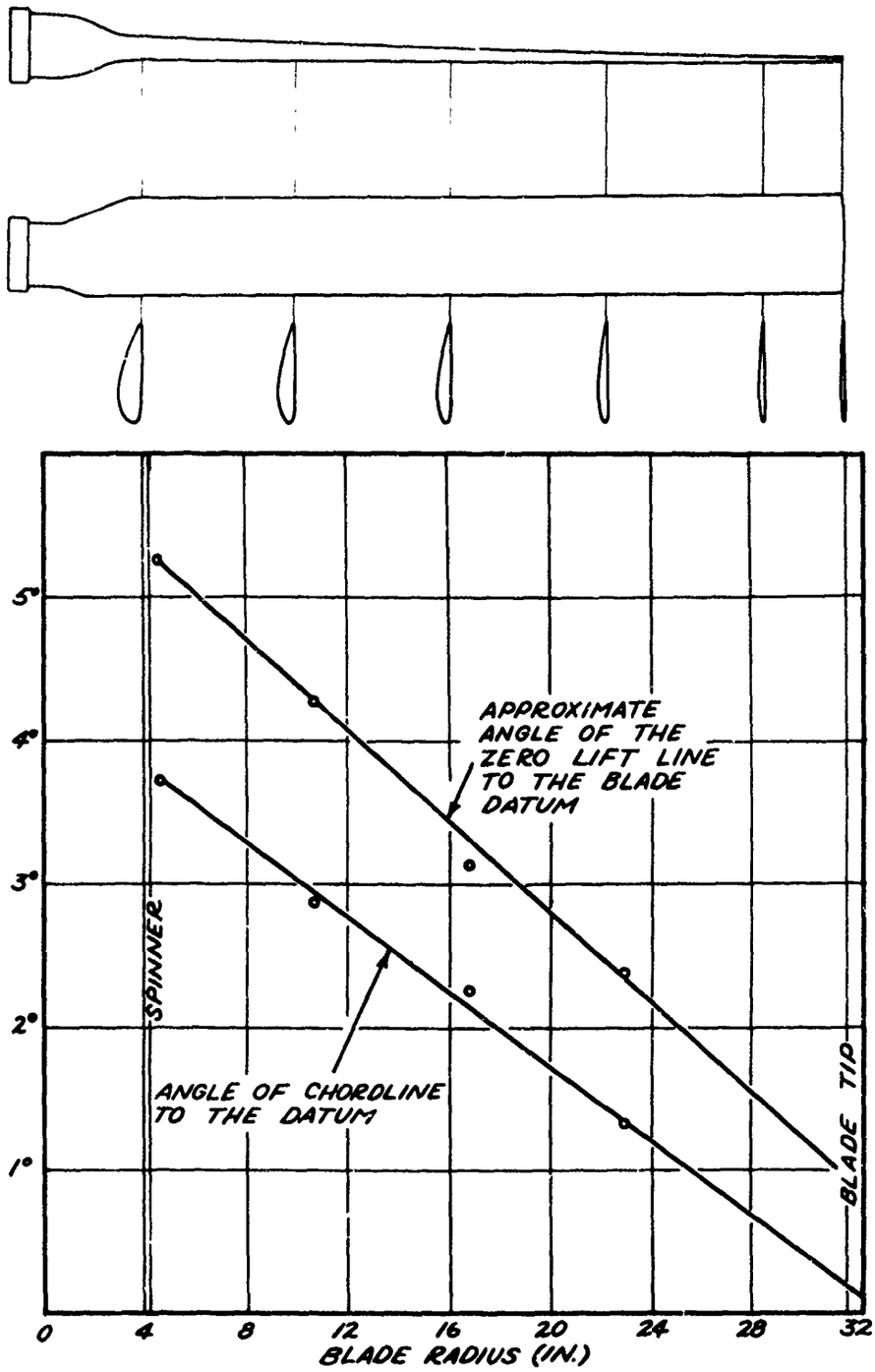

Figure 4. Propeller Drawing Showing Propeller Geometry and Twist Distribution.

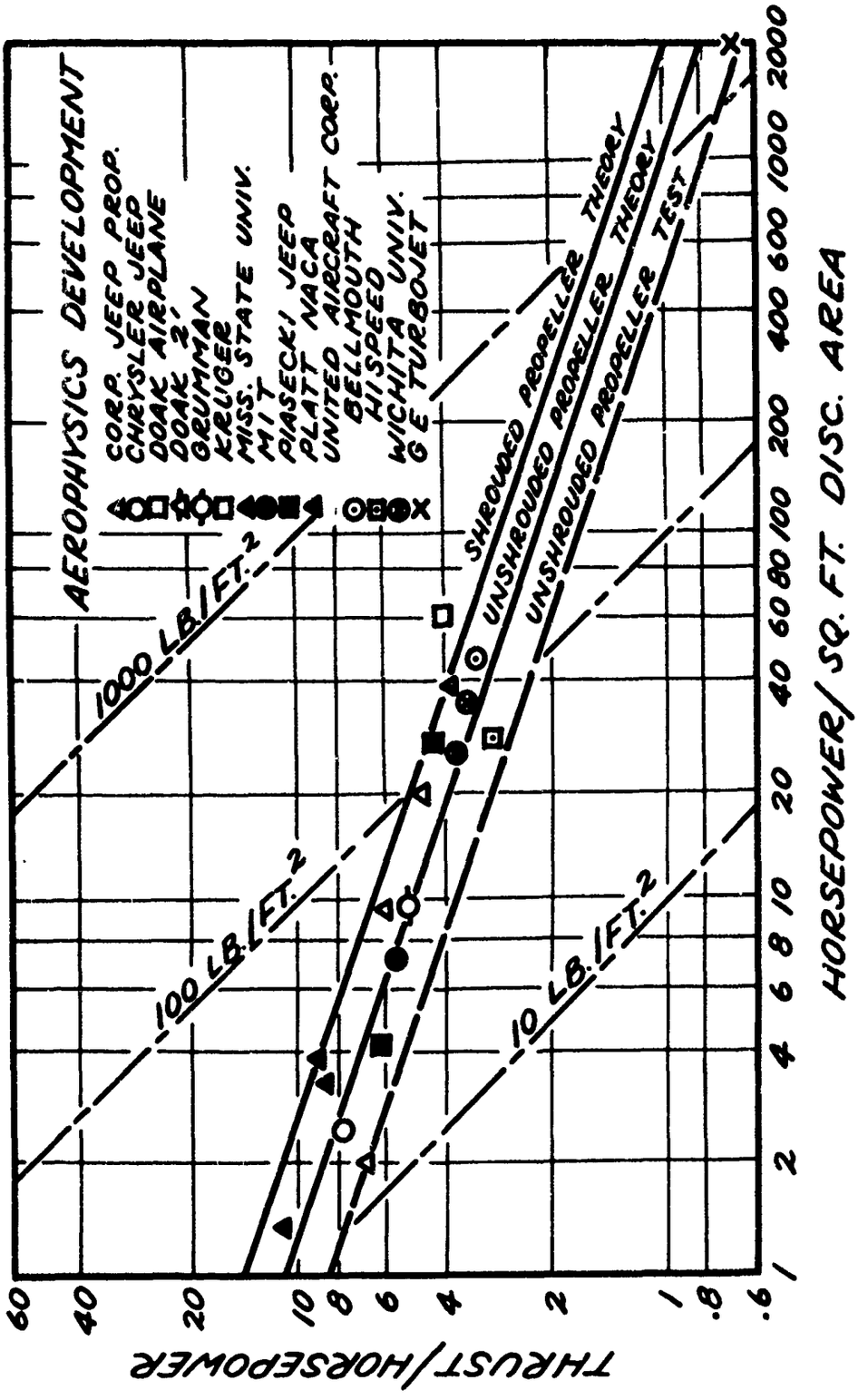

Figure 5. Ducted Propulsor Performance Chart.

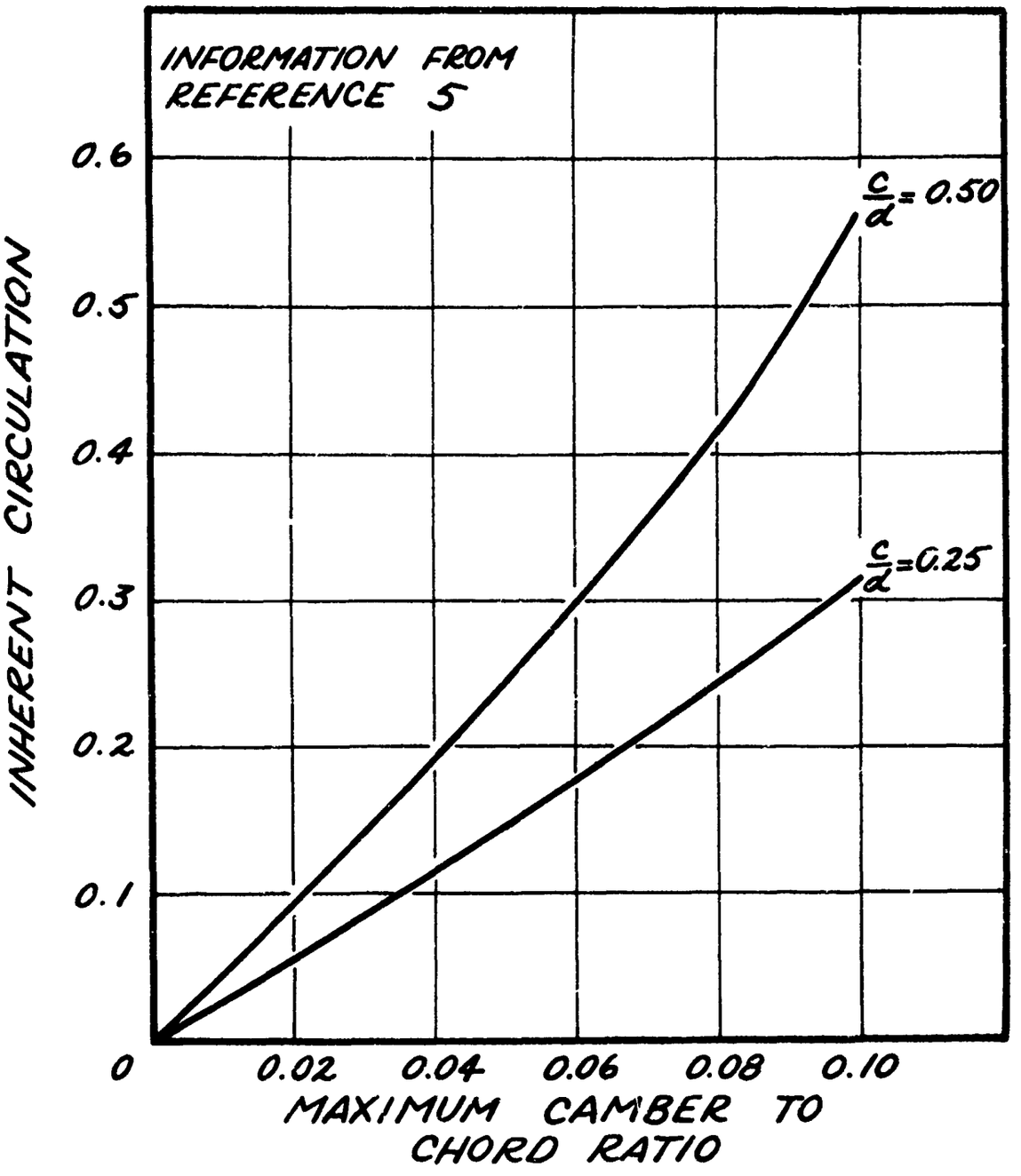

Figure 6. Effect of Shroud Camber on Circulation (Reference 5).

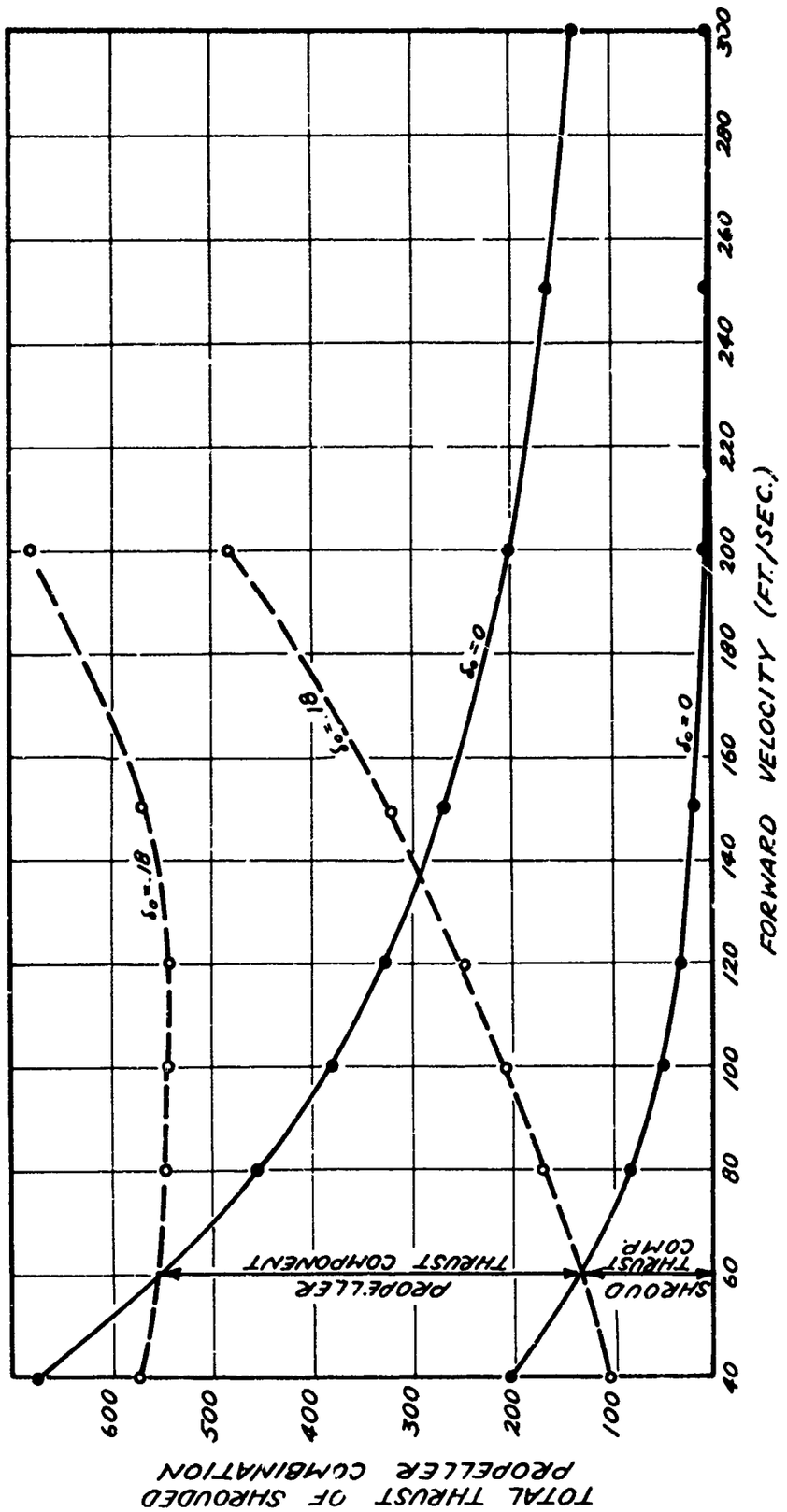

Figure 7. Theoretical Variation of Total Thrust With Forward Velocity for the MARVELETTE Shrouded Propeller.

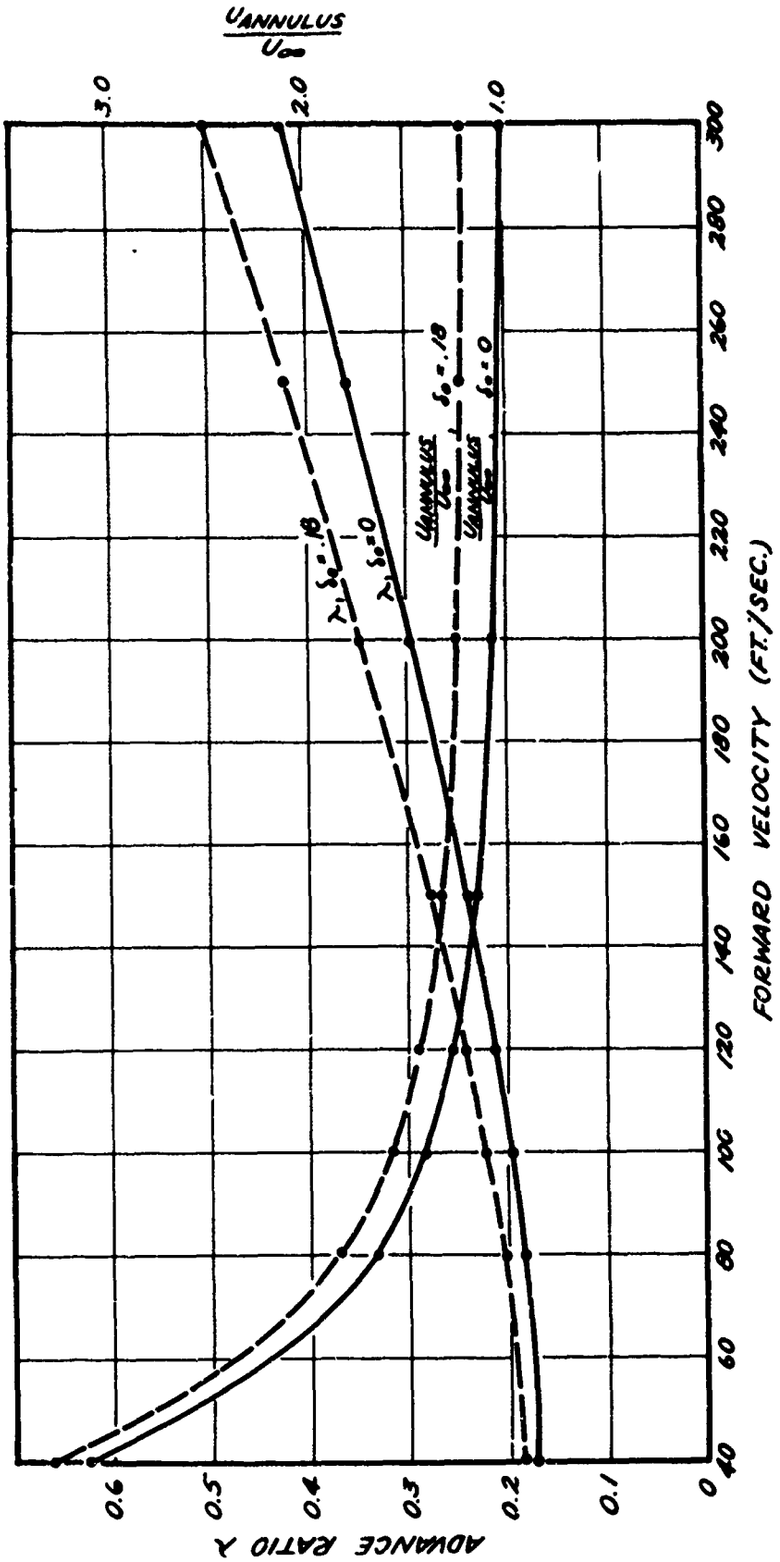

Figure 8. Theoretical Variations of Inflow Velocity and Advance Ratio With Forward Velocity for the MARVELETTE Shrouded Propeller.

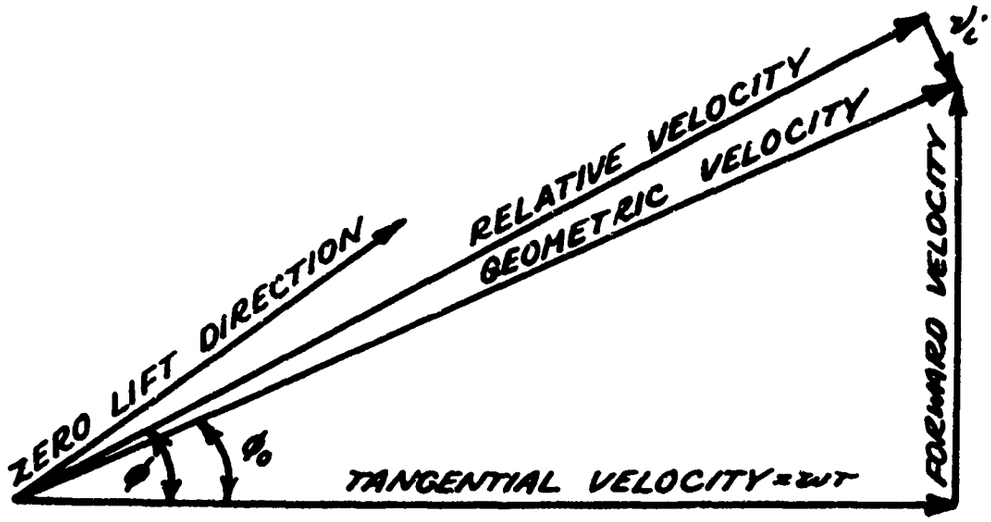

Figure 9. Blade Element Diagrams.

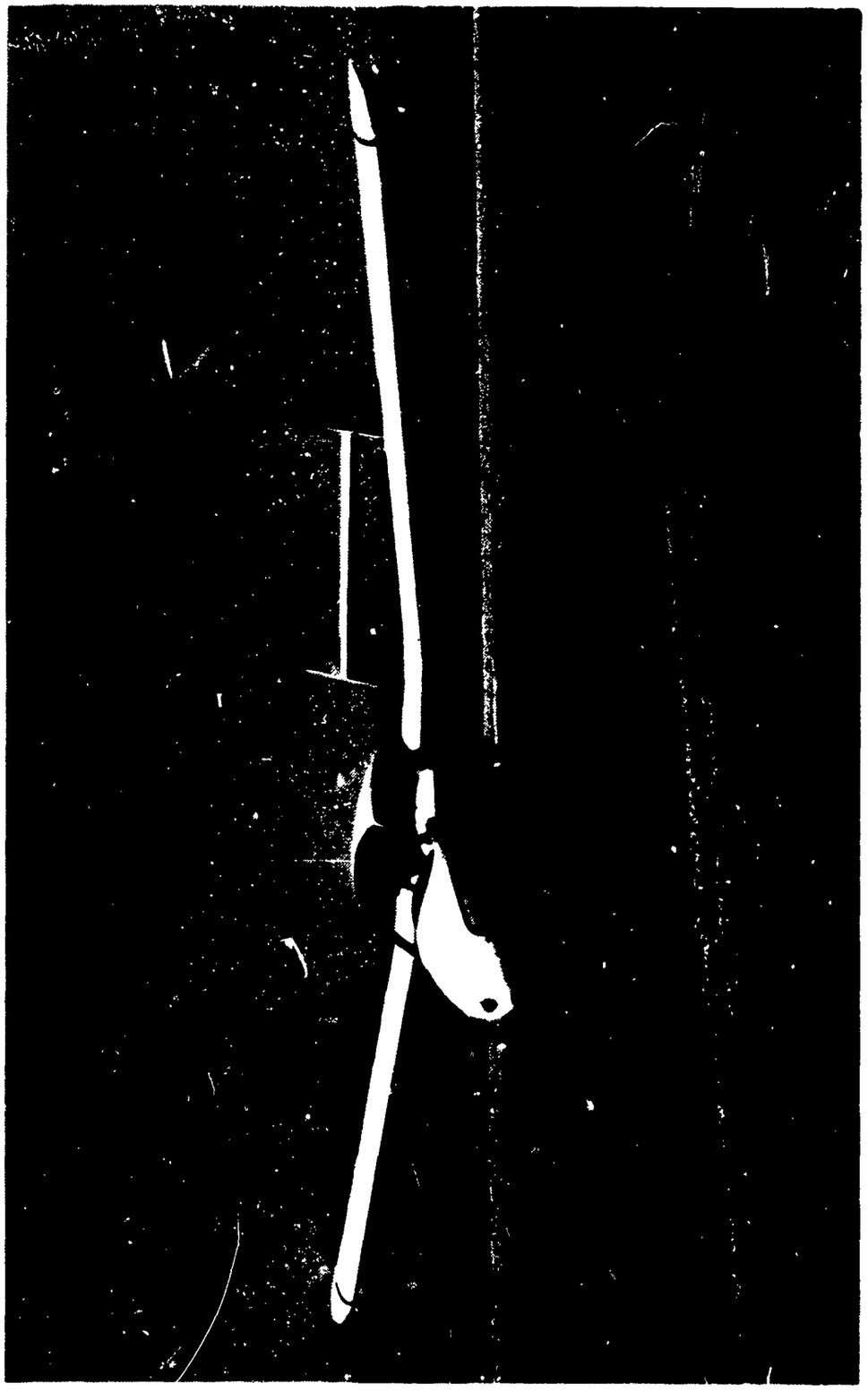

Figure 10. The AG-14.

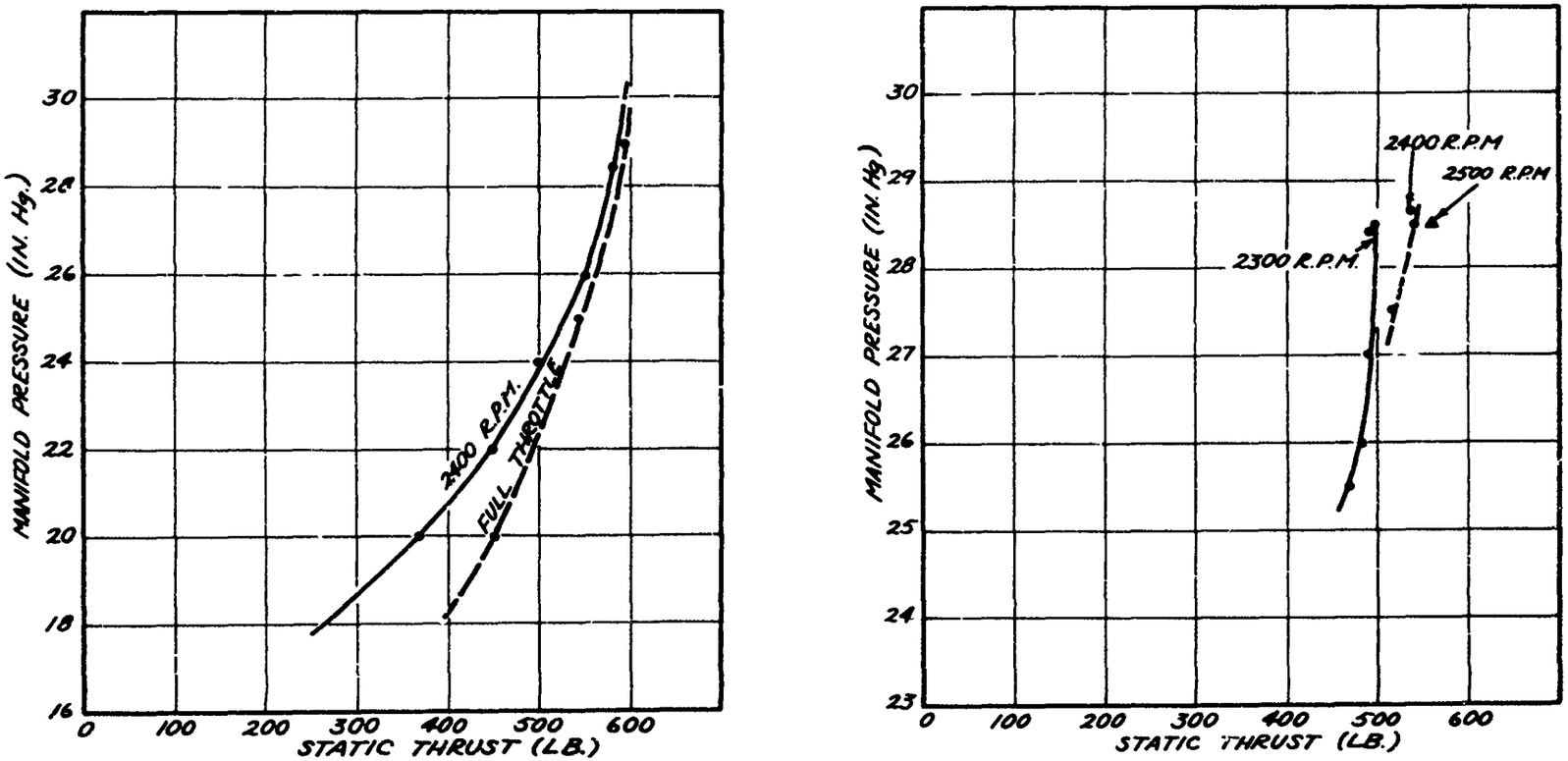

A. Straight Blade

B. Twist Modification

Figure 11. Shrouded Propeller Static Thrust Results.

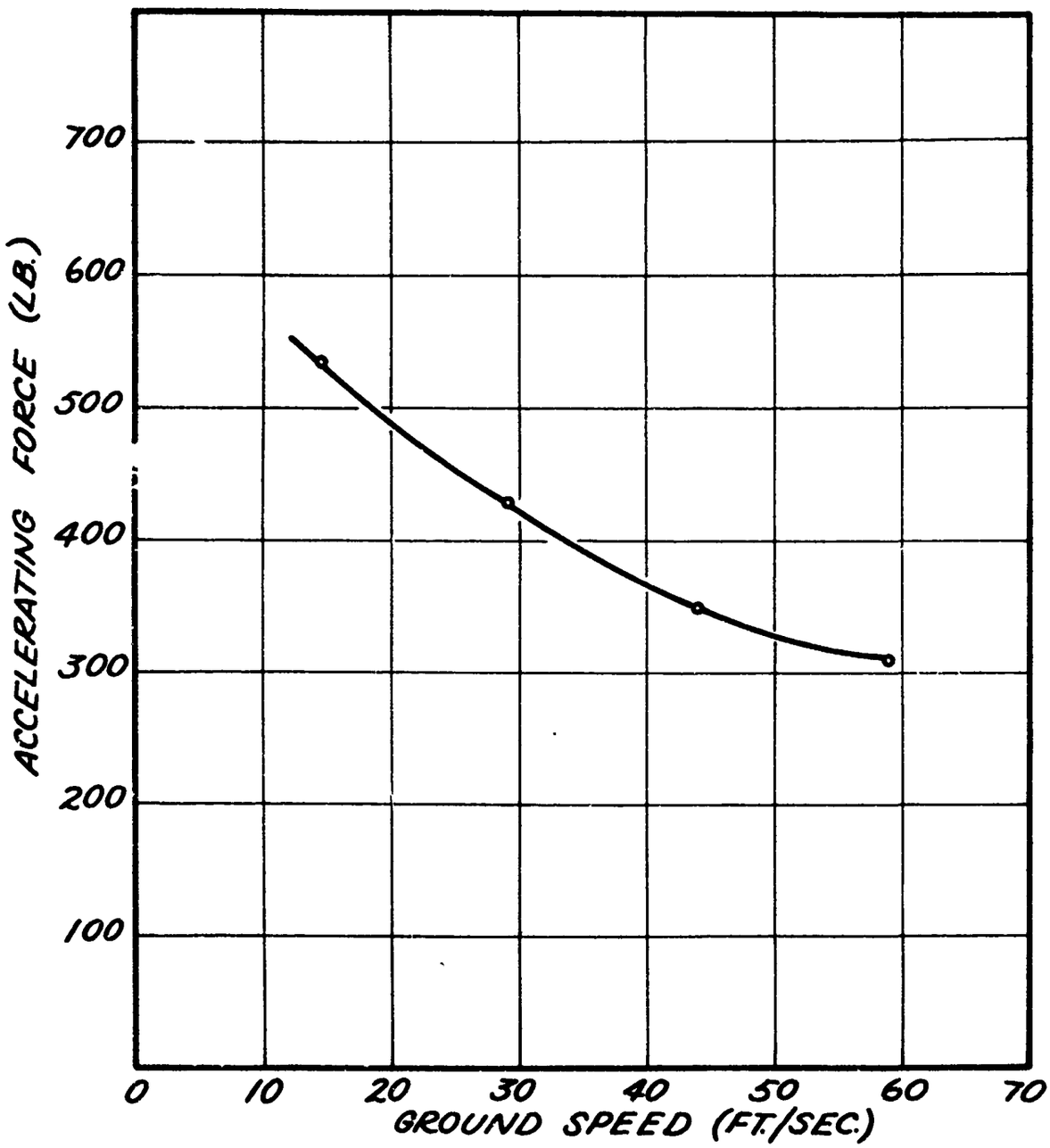

Figure 12. Shrouded Propeller Dynamic Thrust Results, Dragging Tests.

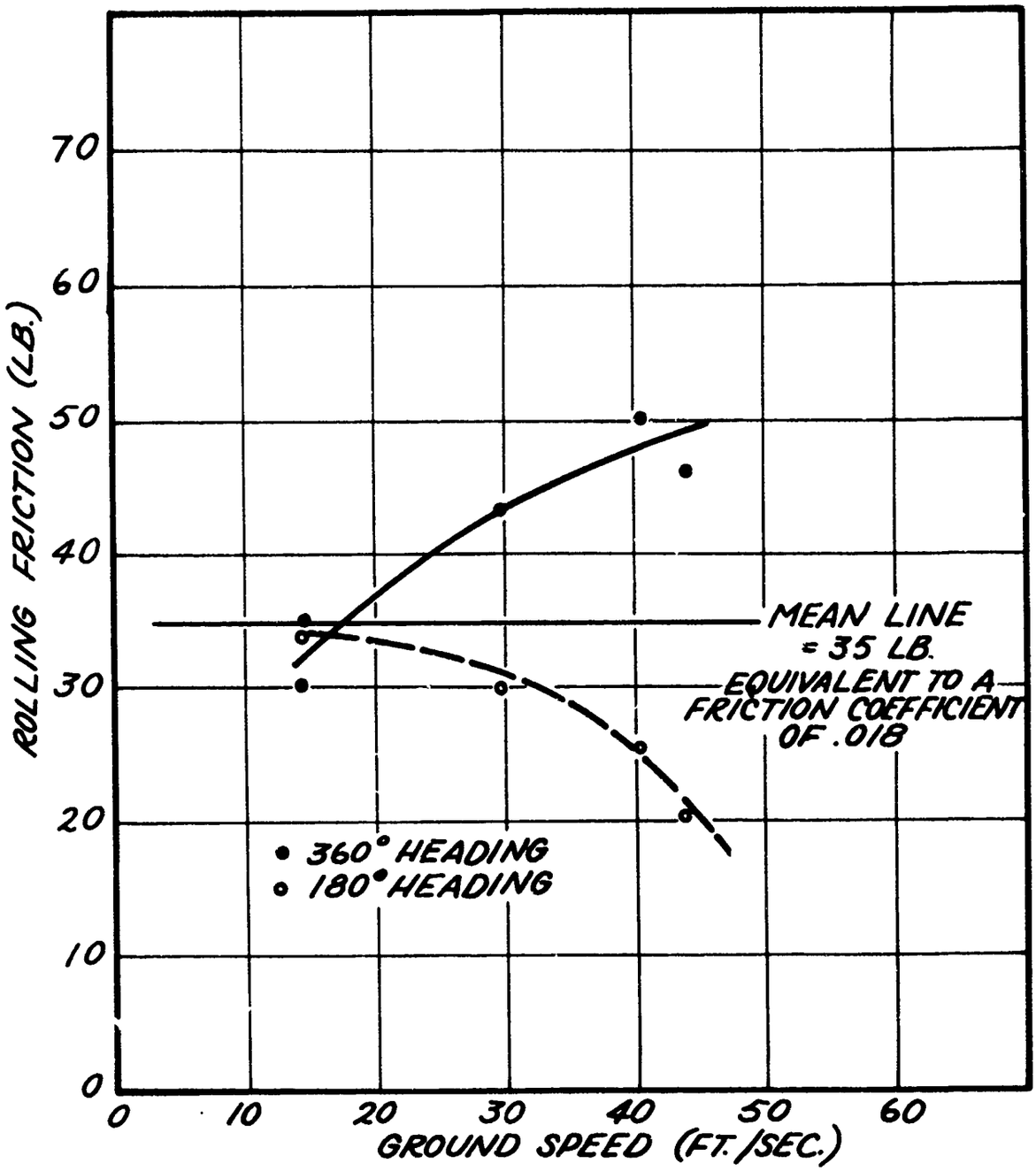

Figure 13. MARVELETTE Rolling Friction Tests.

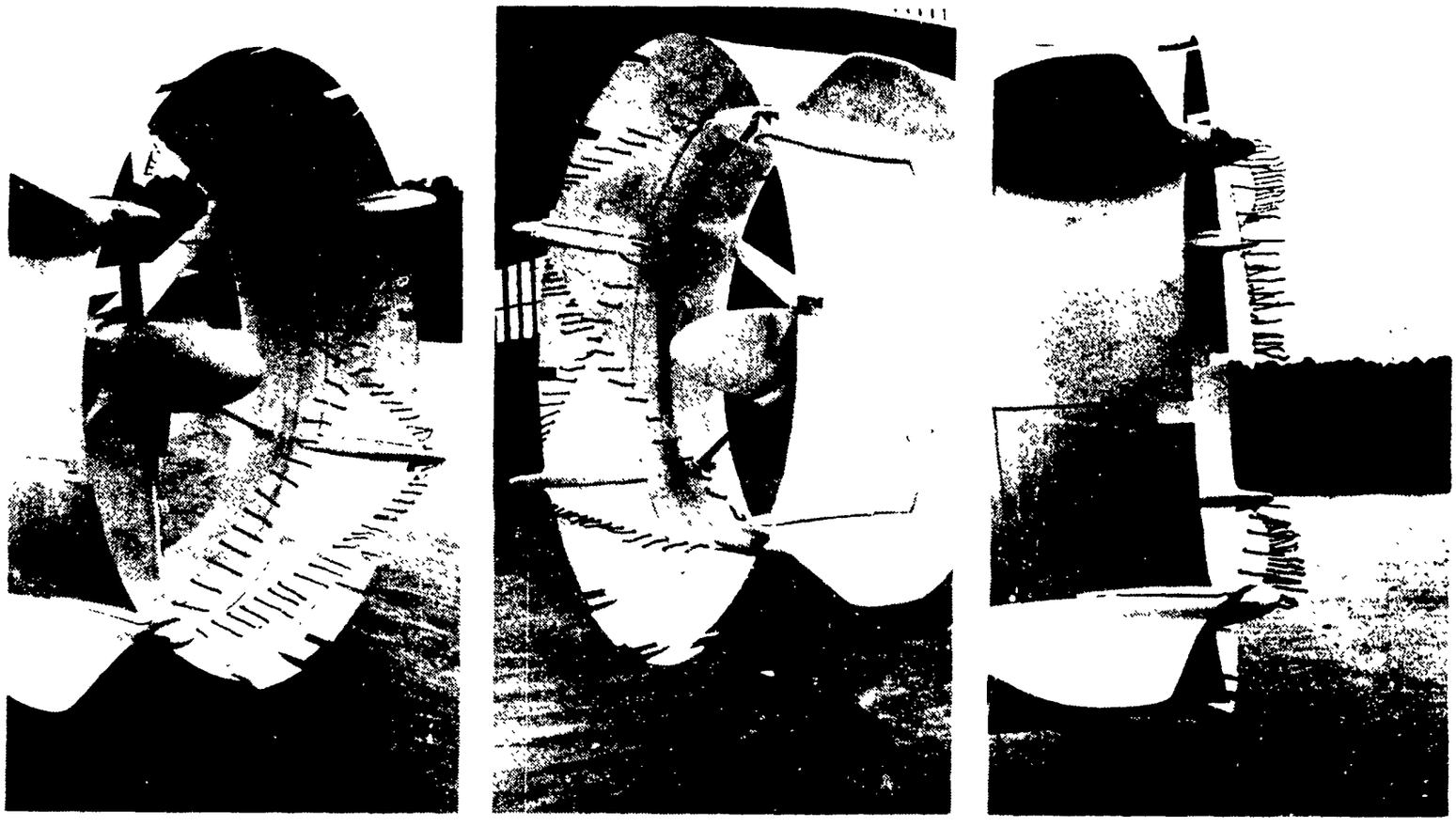

Figure 14A. Tuft Studies of the Shrouded Propeller in the Static Condition, Full Throttle, 2500 R.P.M.

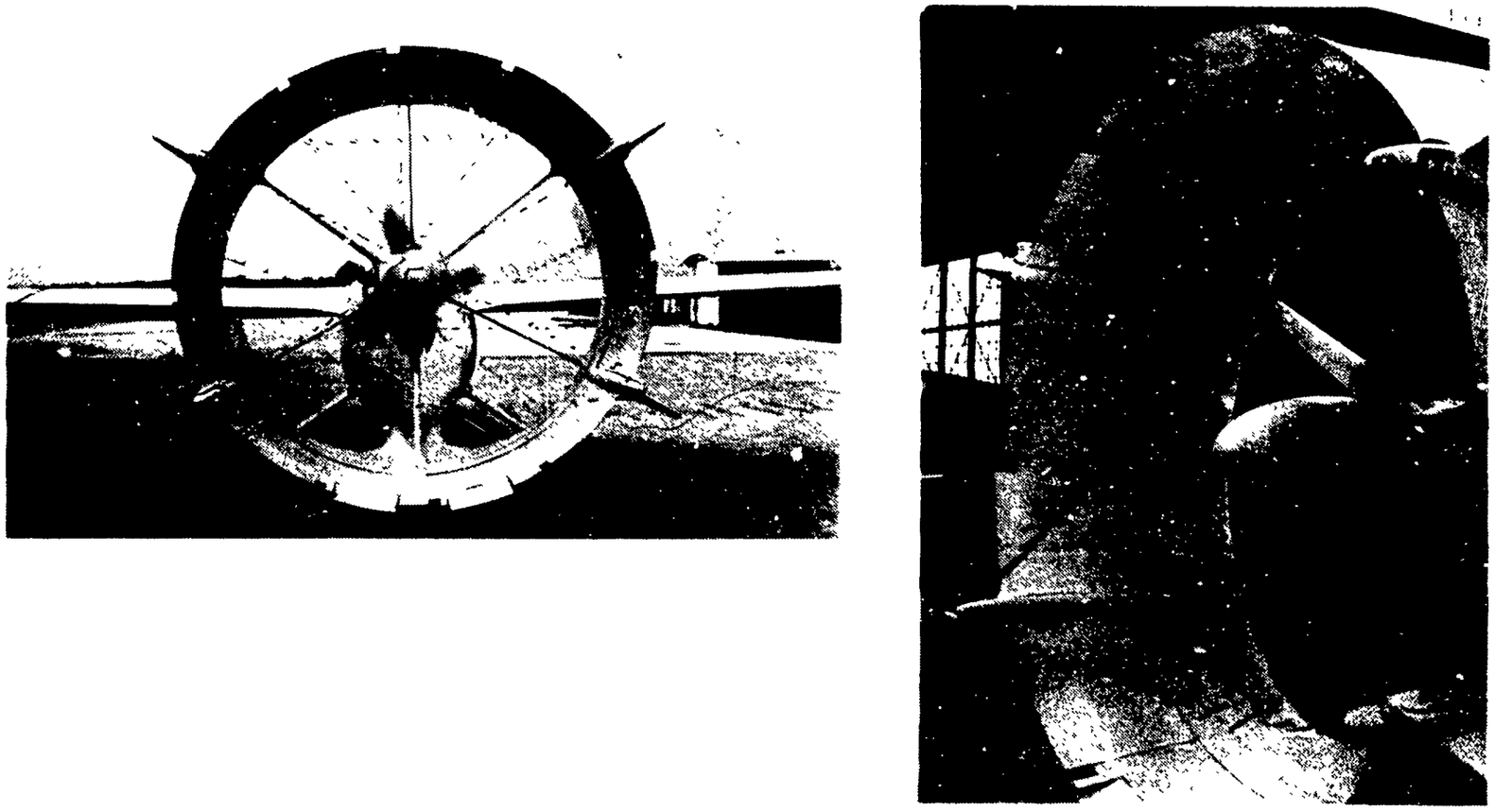

Figure 14B. Tuft Studies of the Shrouded Propeller, Aft of Propeller Plane, in the Static Condition, 2300 R.P.M.

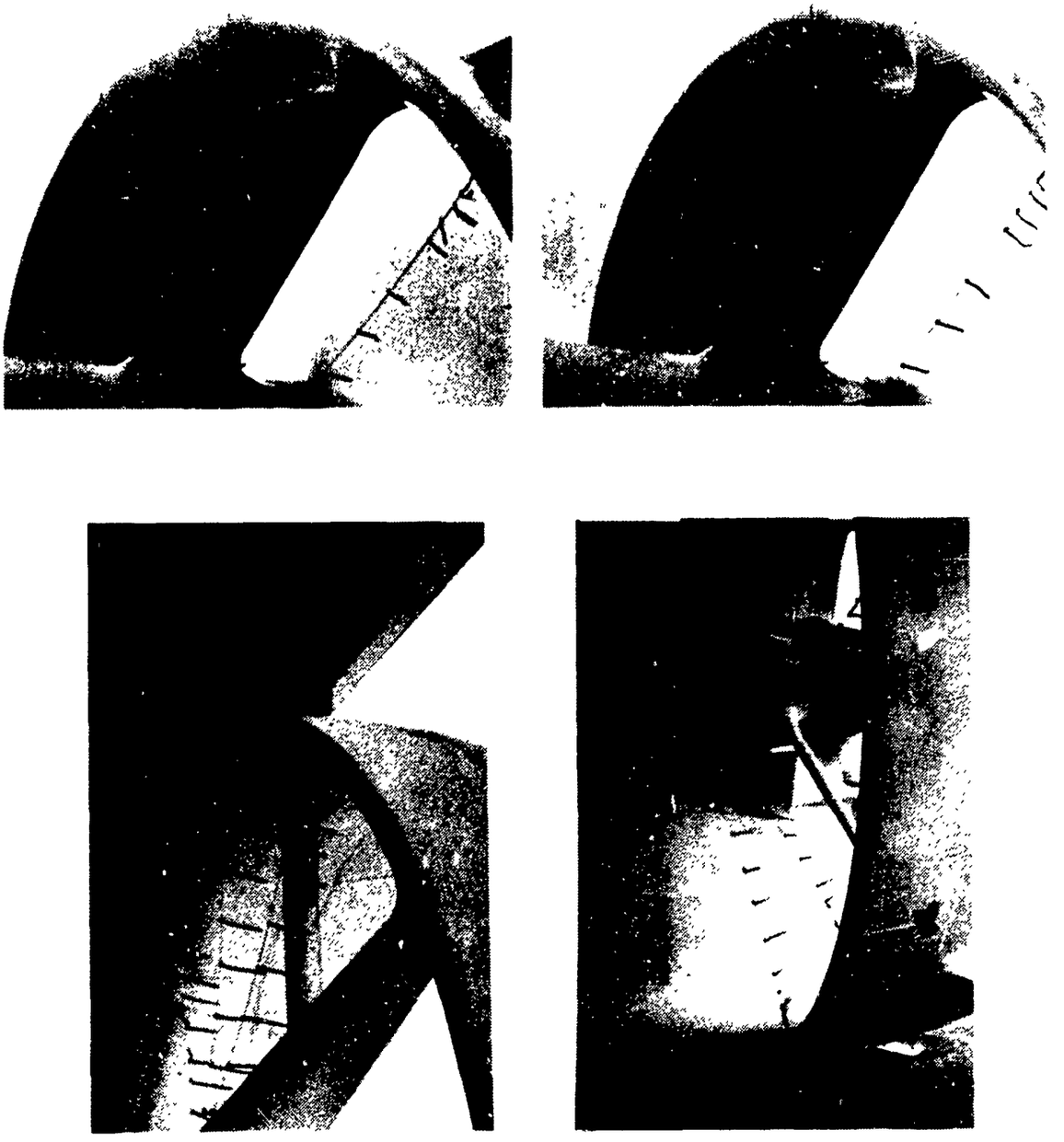

Figure 14C. Tuft Studies of the Shrouded Propeller, Forward of Propeller Plane, in the Static Condition, 2300 R.P.M.

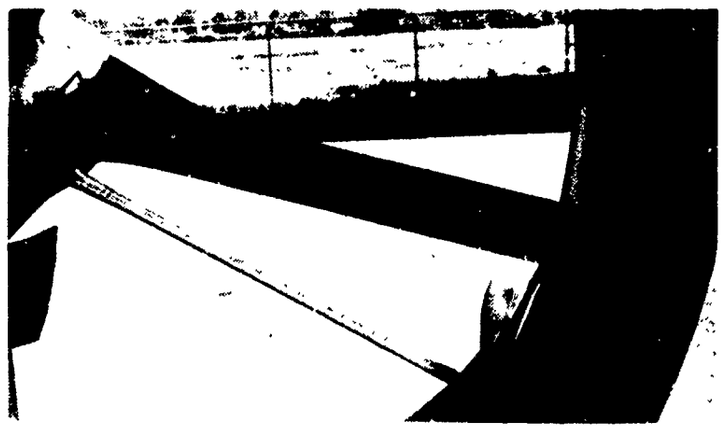

After 5 Seconds

After 10 Seconds

After 15 Seconds

Figure 15A. Sublimation Studies of the Shrouded Propeller, Static Condition, Shroud Leading Edge.

After 10 Seconds

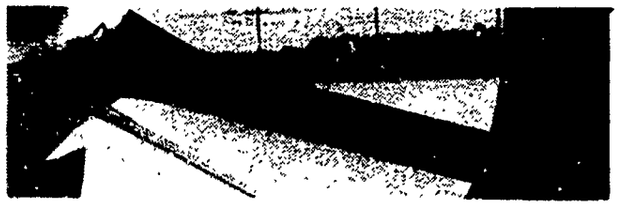

After 15 Seconds

After 20 Seconds

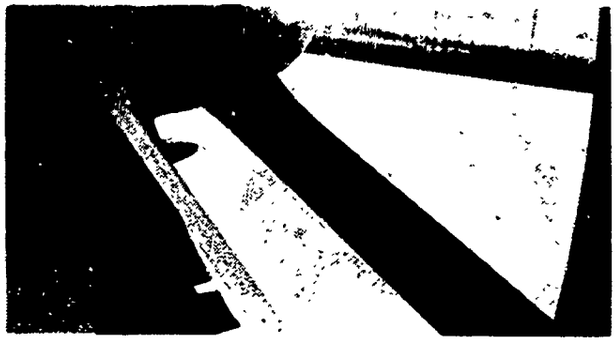

After 30 Seconds

Figure 15B. Sublimation Studies of the Shrouded Propeller, Static Condition, Propeller Blade.

After 2 Runs | After 3 Runs | After 4 Runs | After 5 Runs

Figure 15C. Sublimation Studies of the Shrouded Propeller, Dynamic Condition, Shroud Leading Edge.

After 1 Run

After 2 Runs

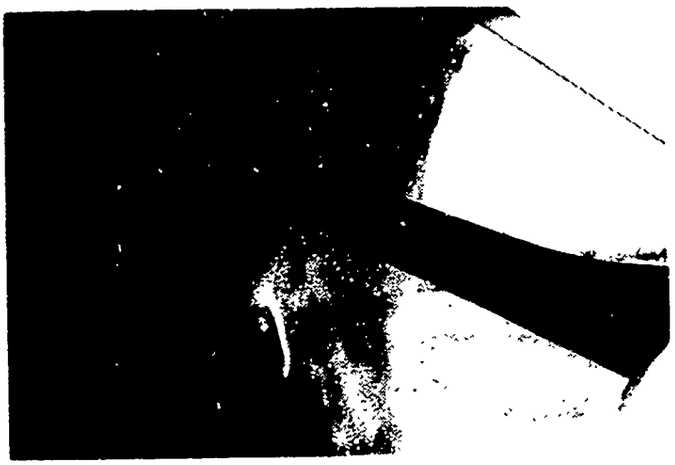

After 5 Runs

Figure 15D. Sublimation Studies of the Shrouded Propeller, Dynamic Condition, Propeller Blade.

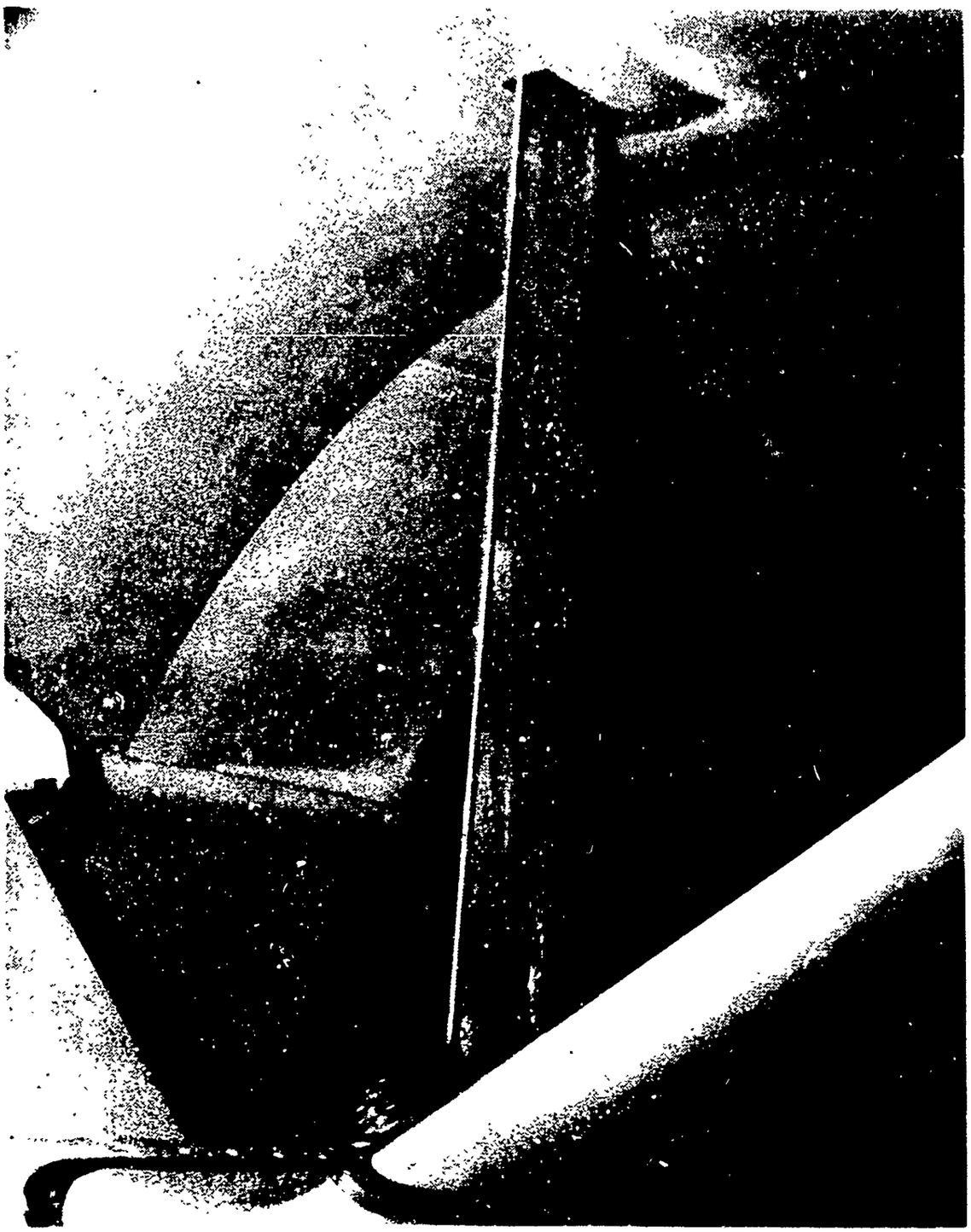

Figure 16. Propeller Inflow Measuring Rake.

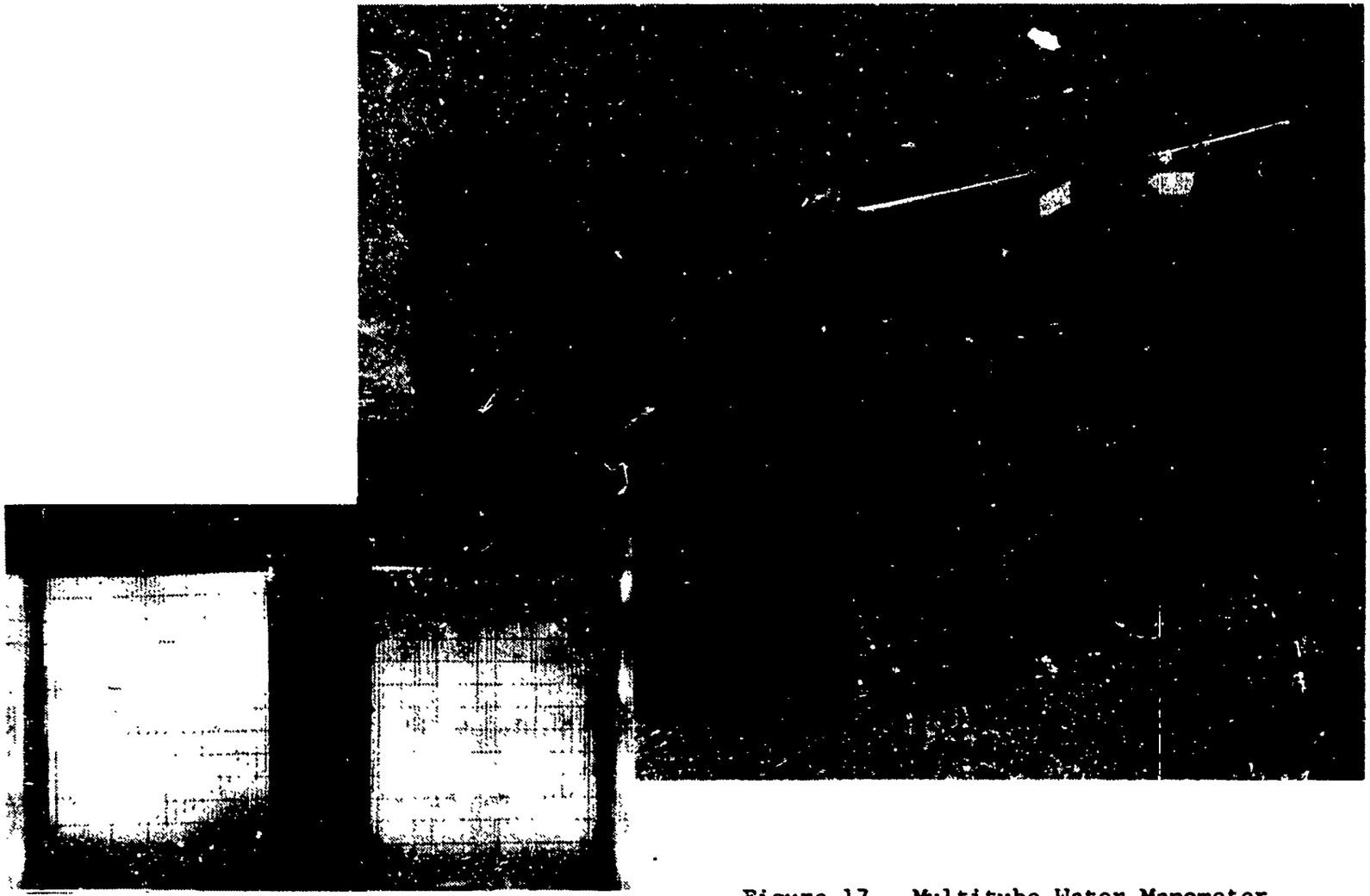

Figure 17. Multitube Water Manometer.

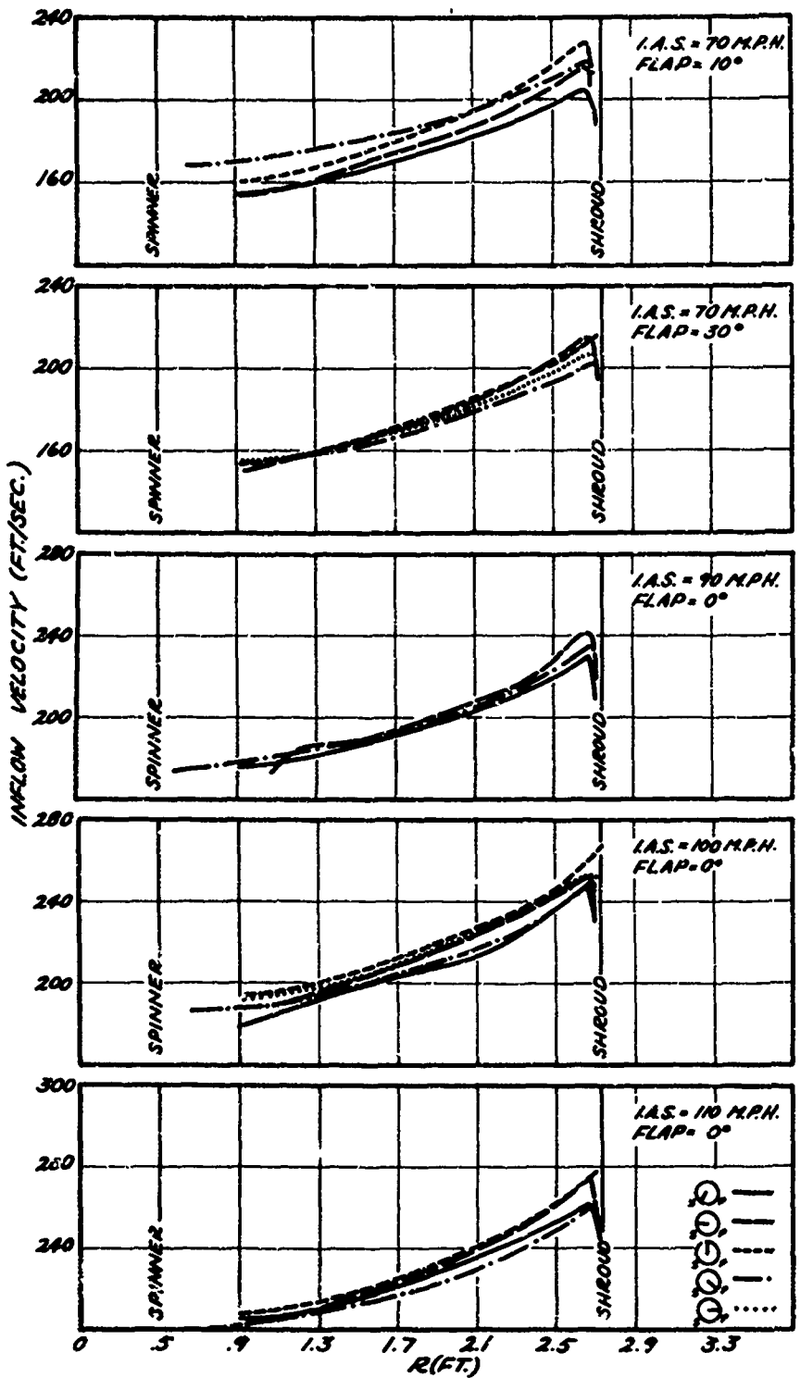

Figure 18. Inflow Measurements at Various Angular Positions in the Shroud Obtained From Flight Tests.

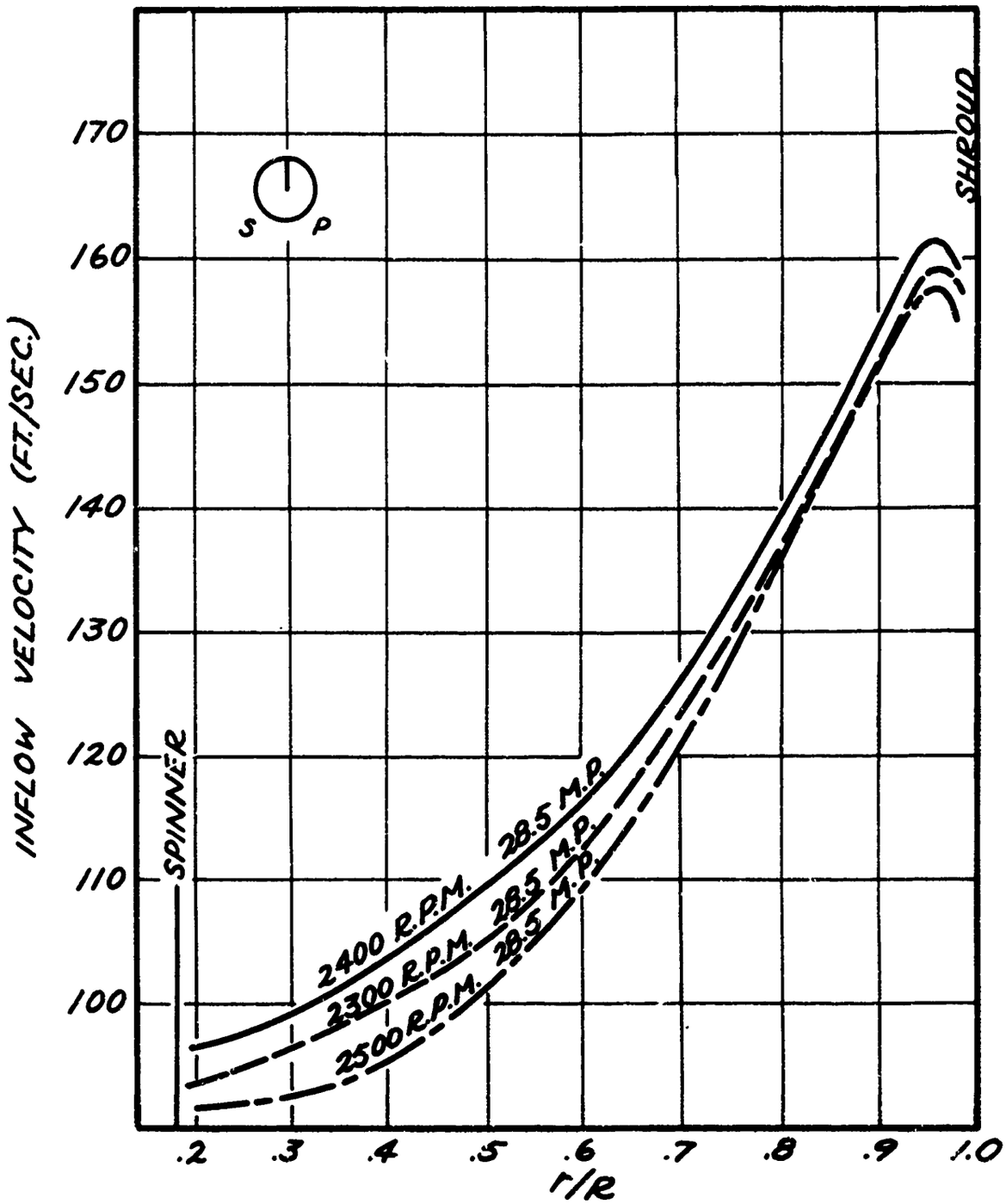

Figure 19. Inflow Measurements in the Top Position for the Static Case.

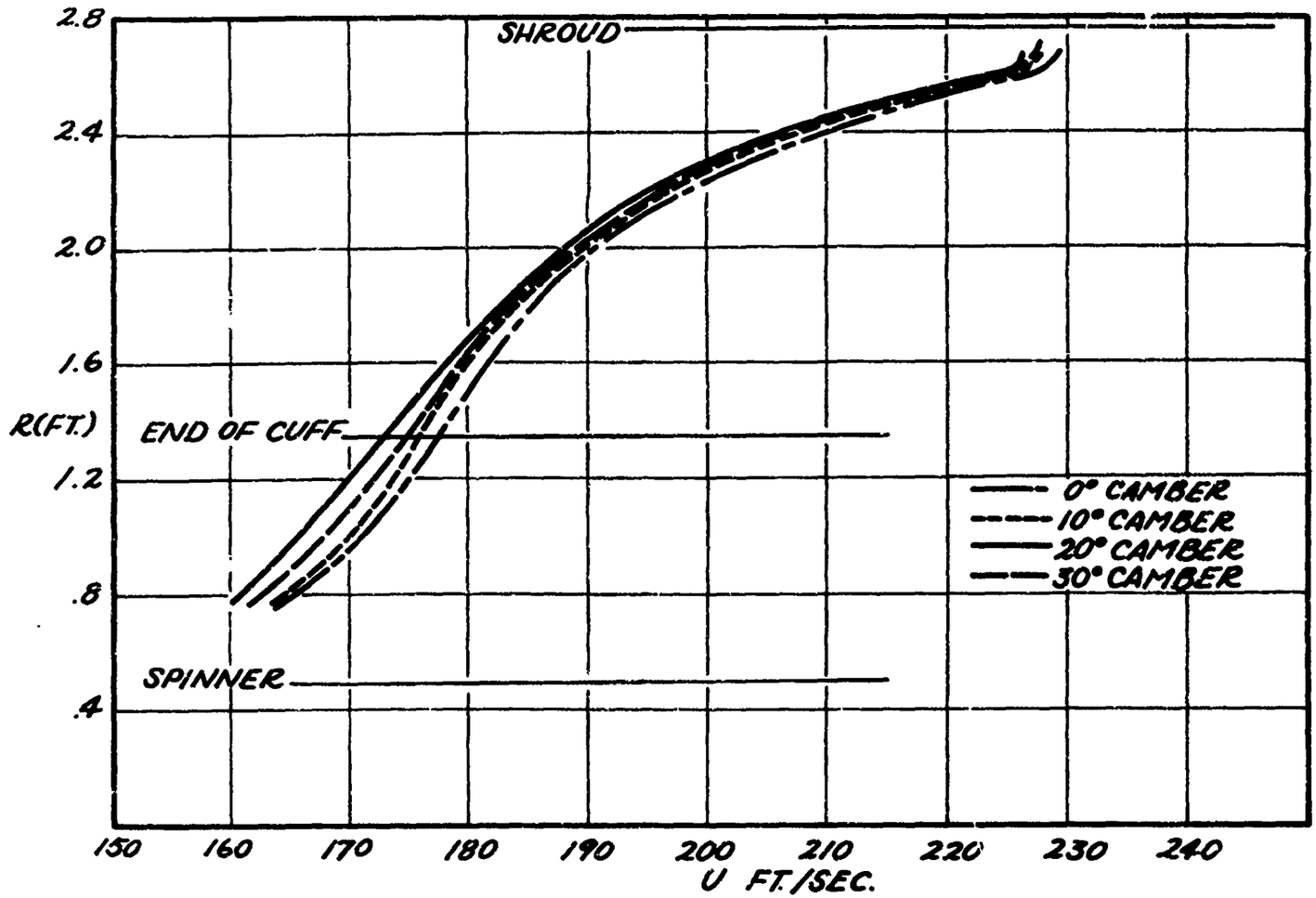

Figure 20. Effect of Equivalent Flap Angle on the Propeller Inflow Velocity at a Constant Aircraft Lift Coefficient.

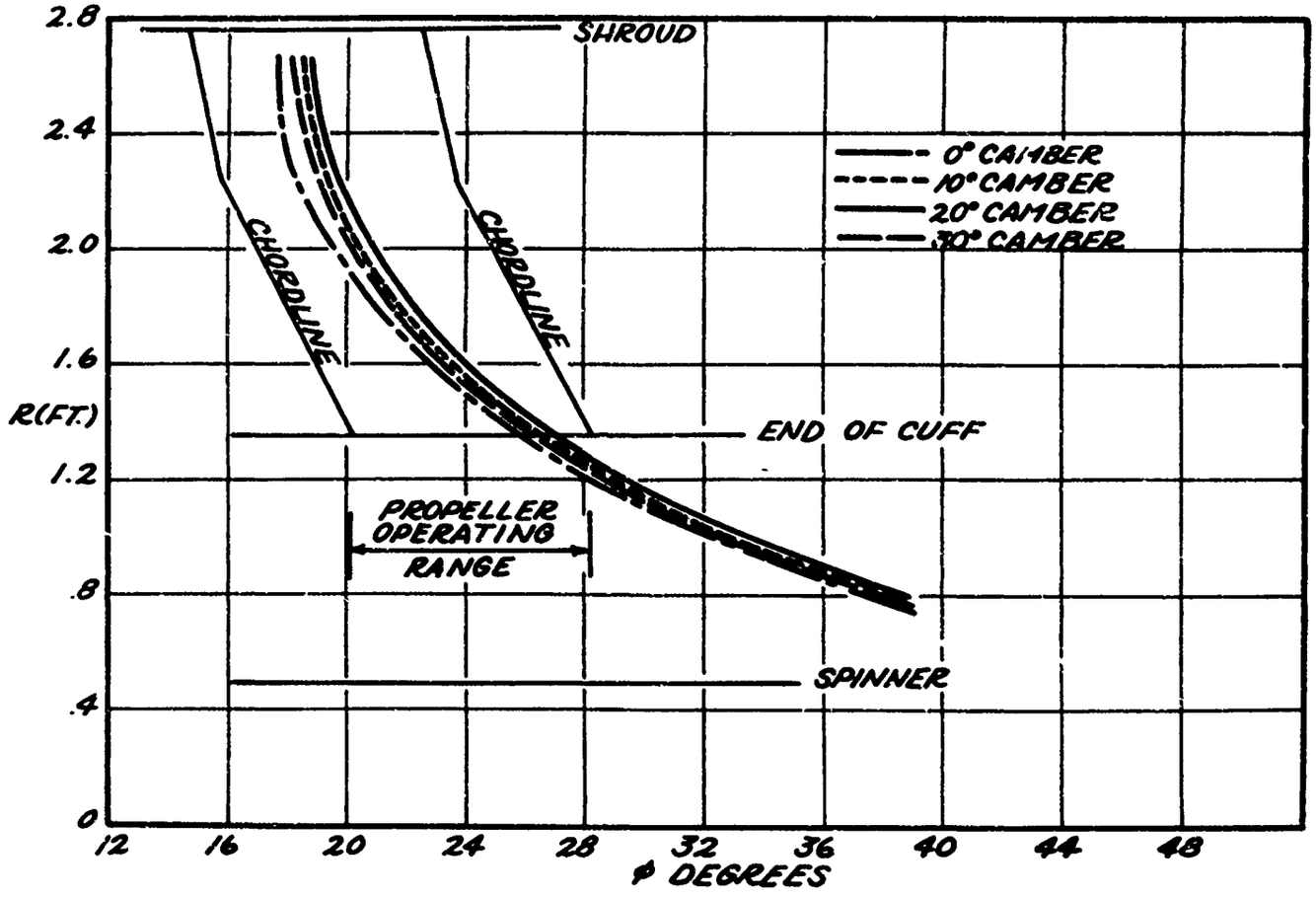

Figure 21. Effect of Equivalent Flap Angle on the Propeller Inflow Angle, ϕ , at a Constant Aircraft Lift Coefficient.

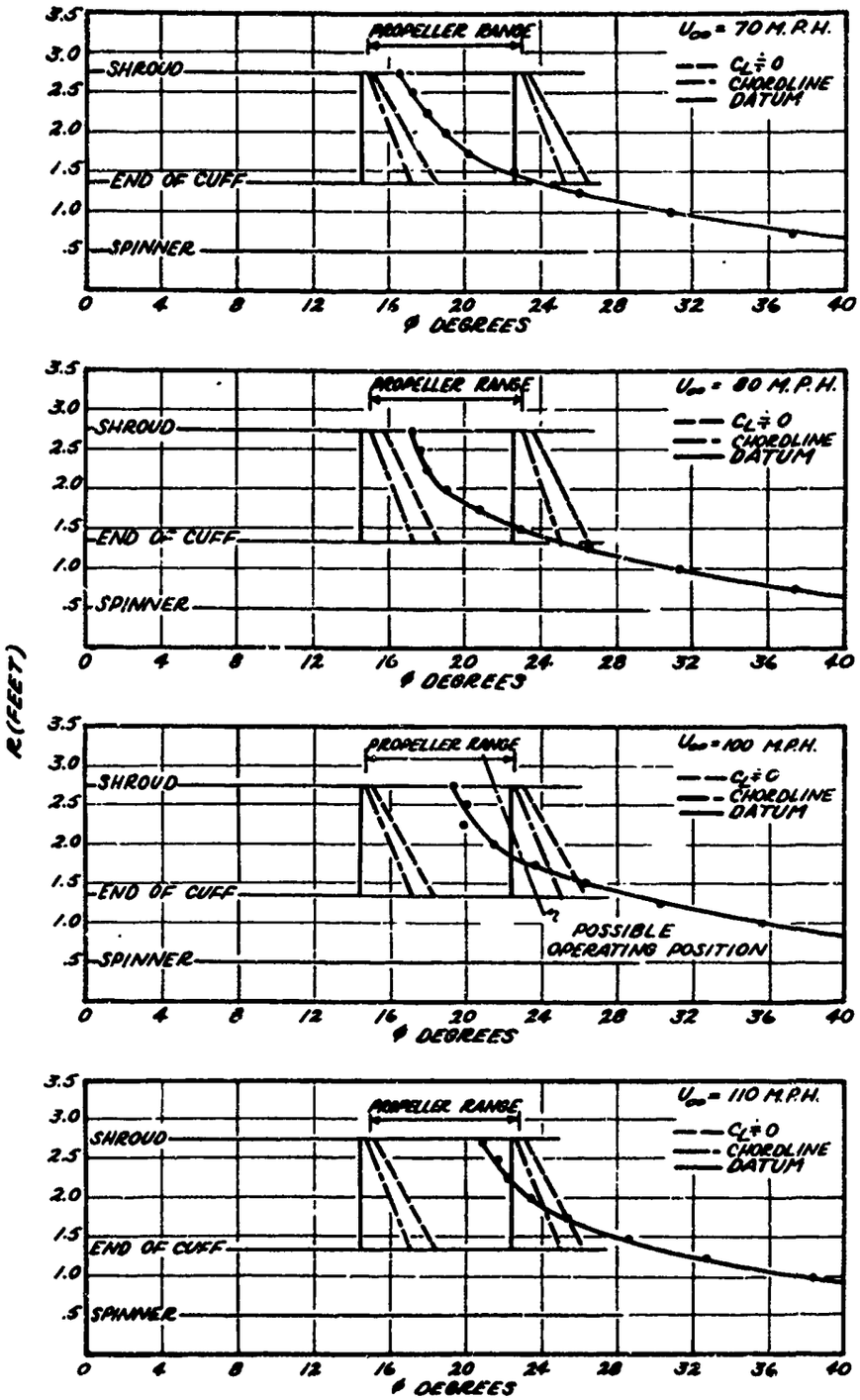

Figure 22A. Effect of Forward Velocity on the Inflow Angle of the Propeller, ϕ, Untwisted Propeller Blades.

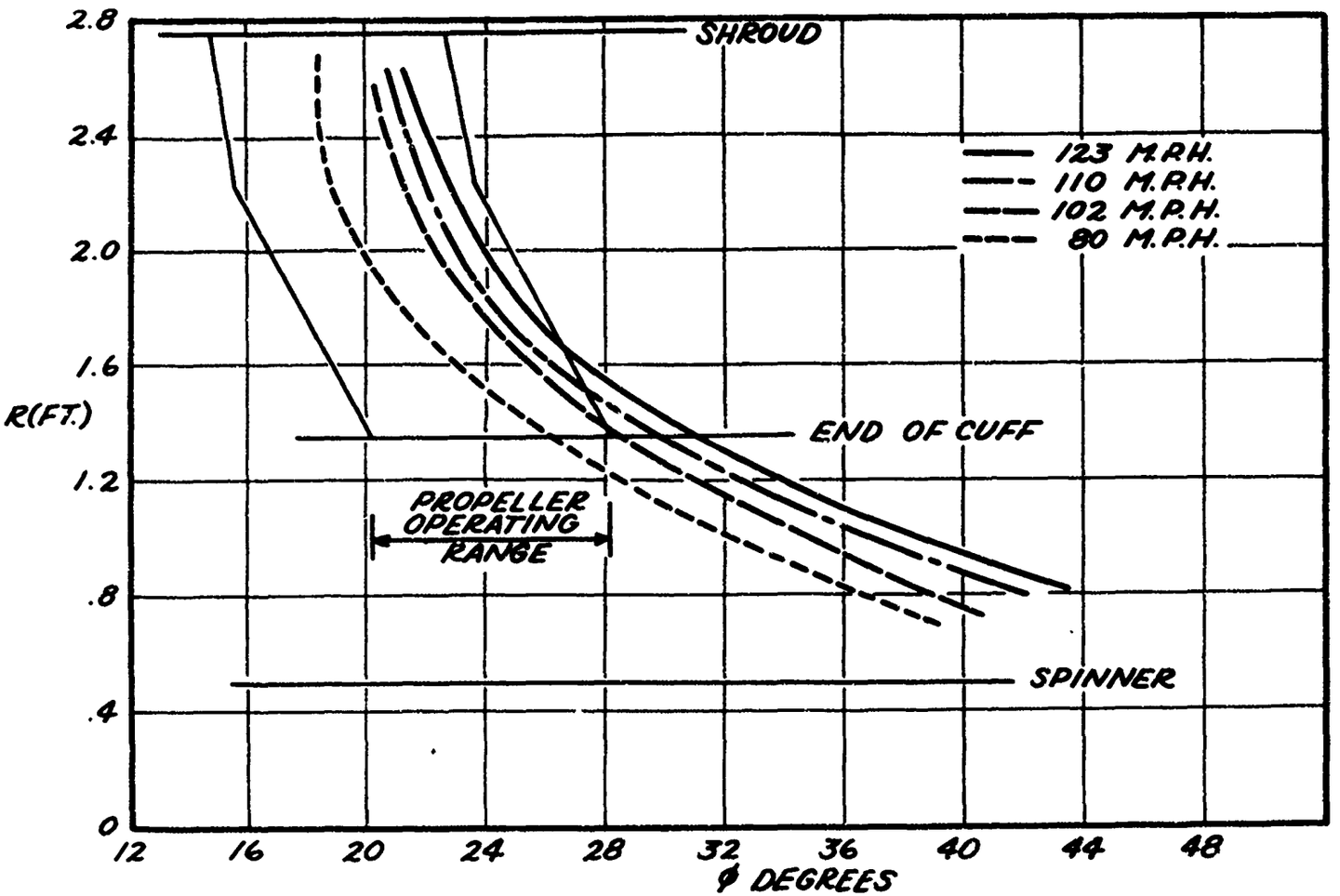

Figure 22B. Effect of Forward Velocity on the Inflow Angle of the Propeller, ϕ , Twisted Propeller Blades.

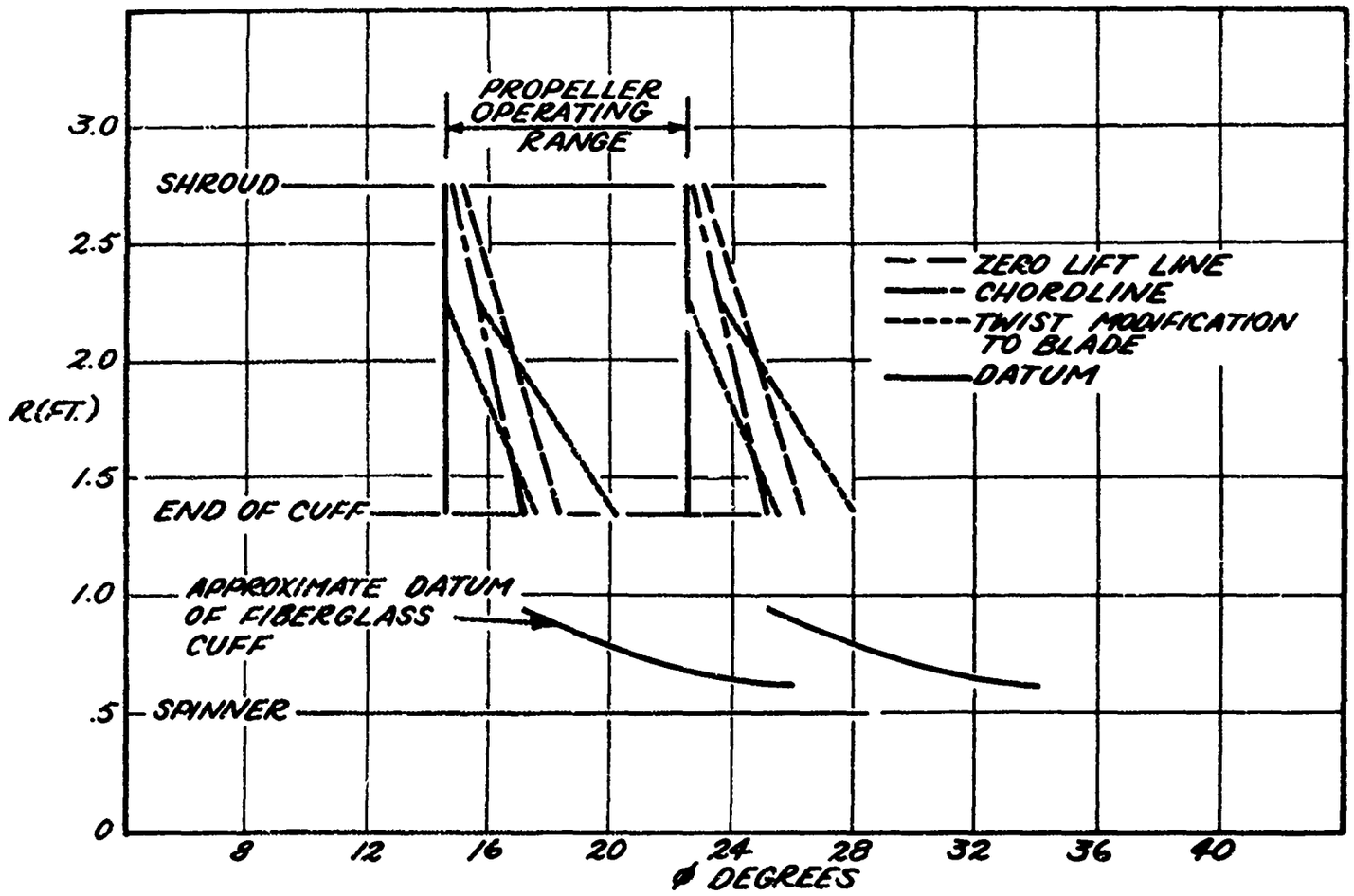

Figure 23. Twist Modification to the MARVELETTE Shrouded Propeller.

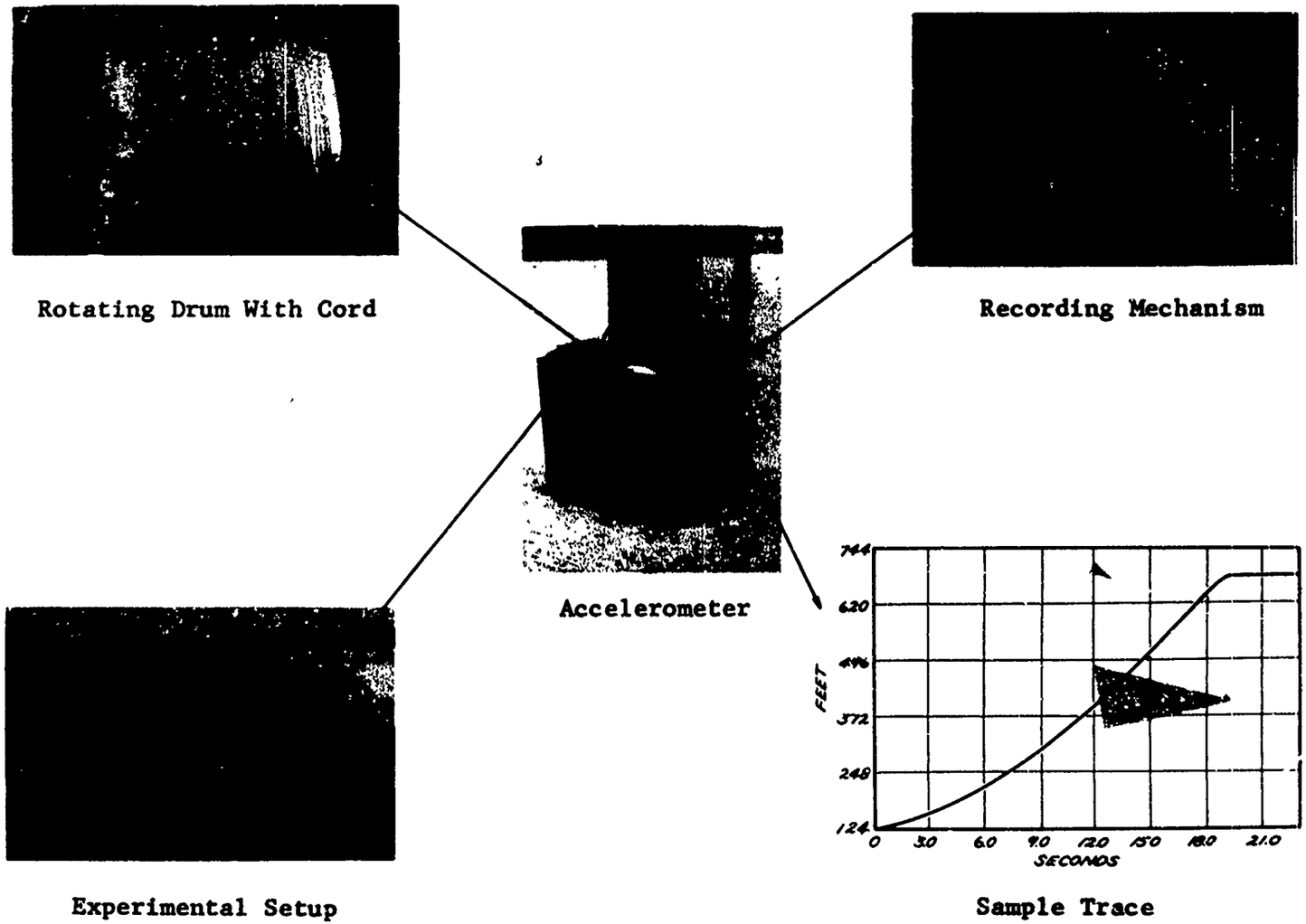

Figure 24. Apparatus Used To Determine Acceleration.

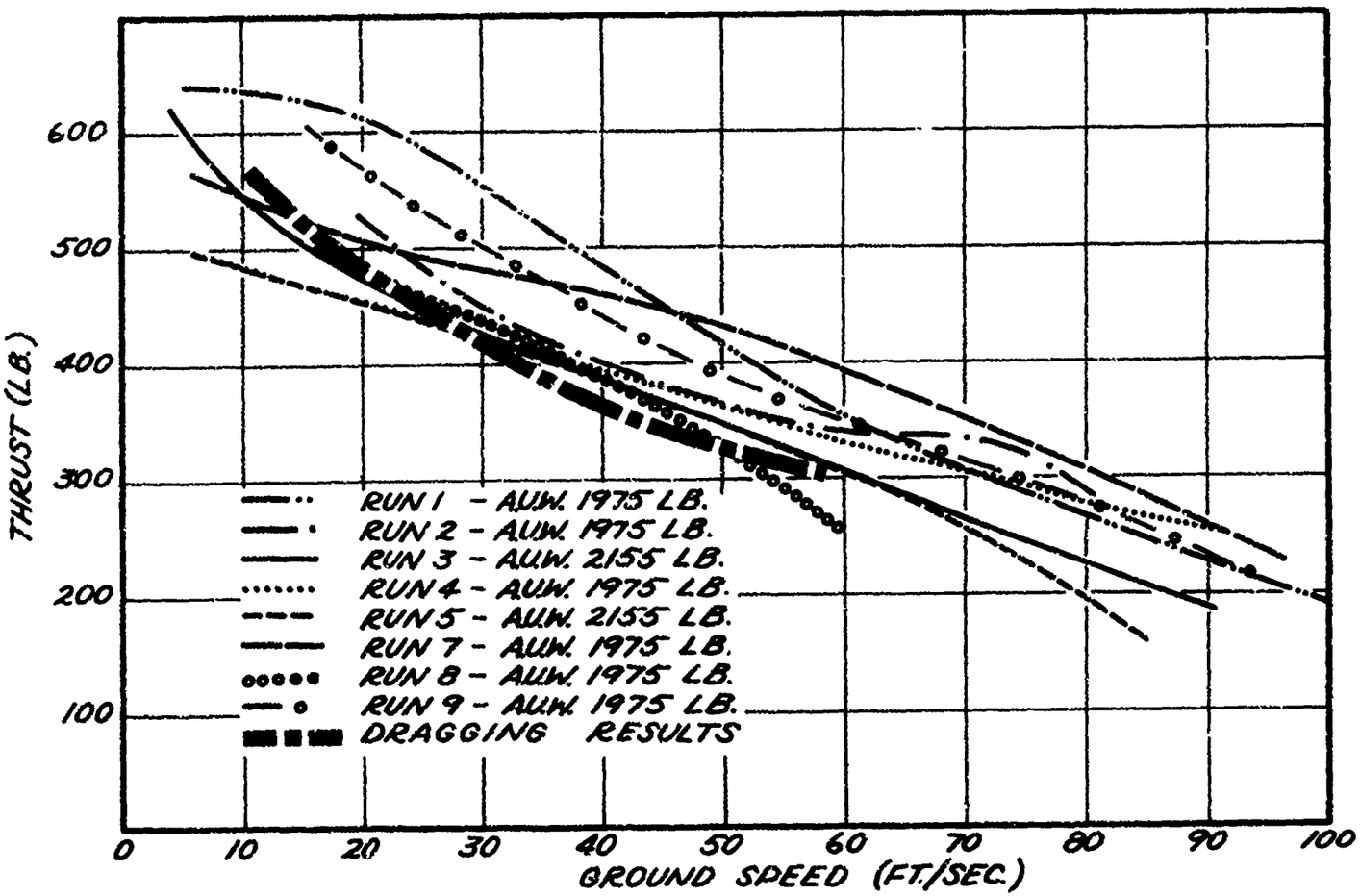

Figure 25. Curves of Thrust Available for Acceleration up to Ground Speeds of 100 Feet Per Second for the MARVELETTE Aircraft.

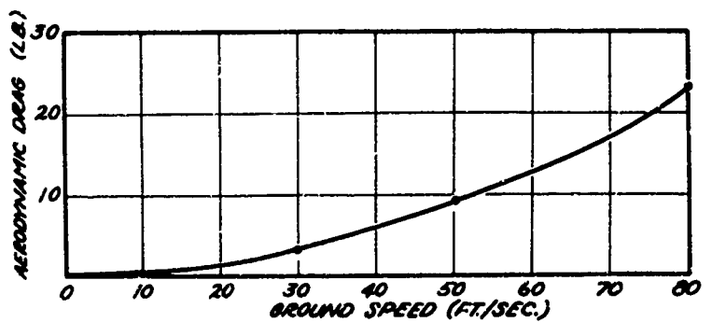

A. Ground Run Assuming a Constant Angle of Attack

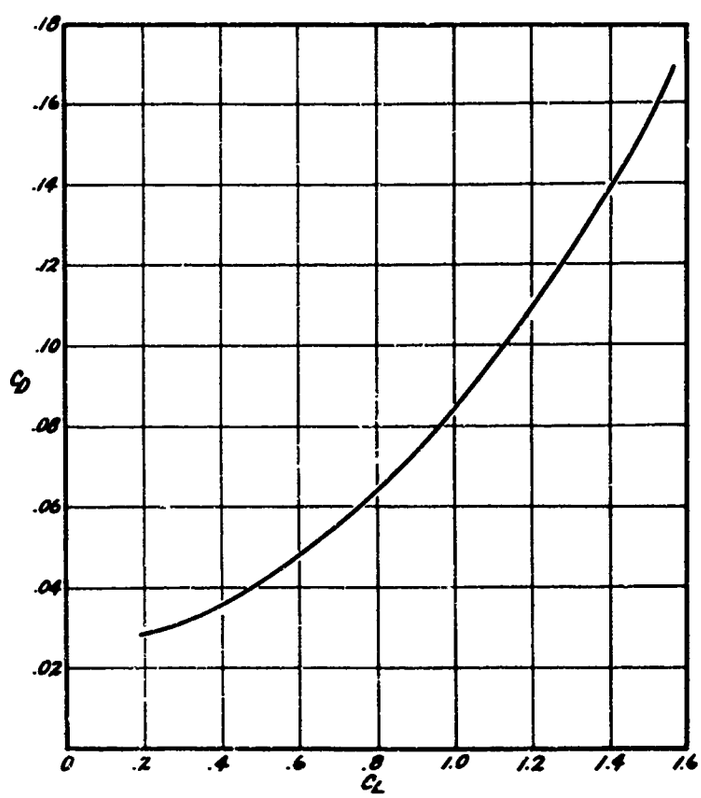

B. Flight Condition, Zero Flap Angle

Figure 26. Estimated Aerodynamic Drag Curves for the MARVELETTE Aircraft.

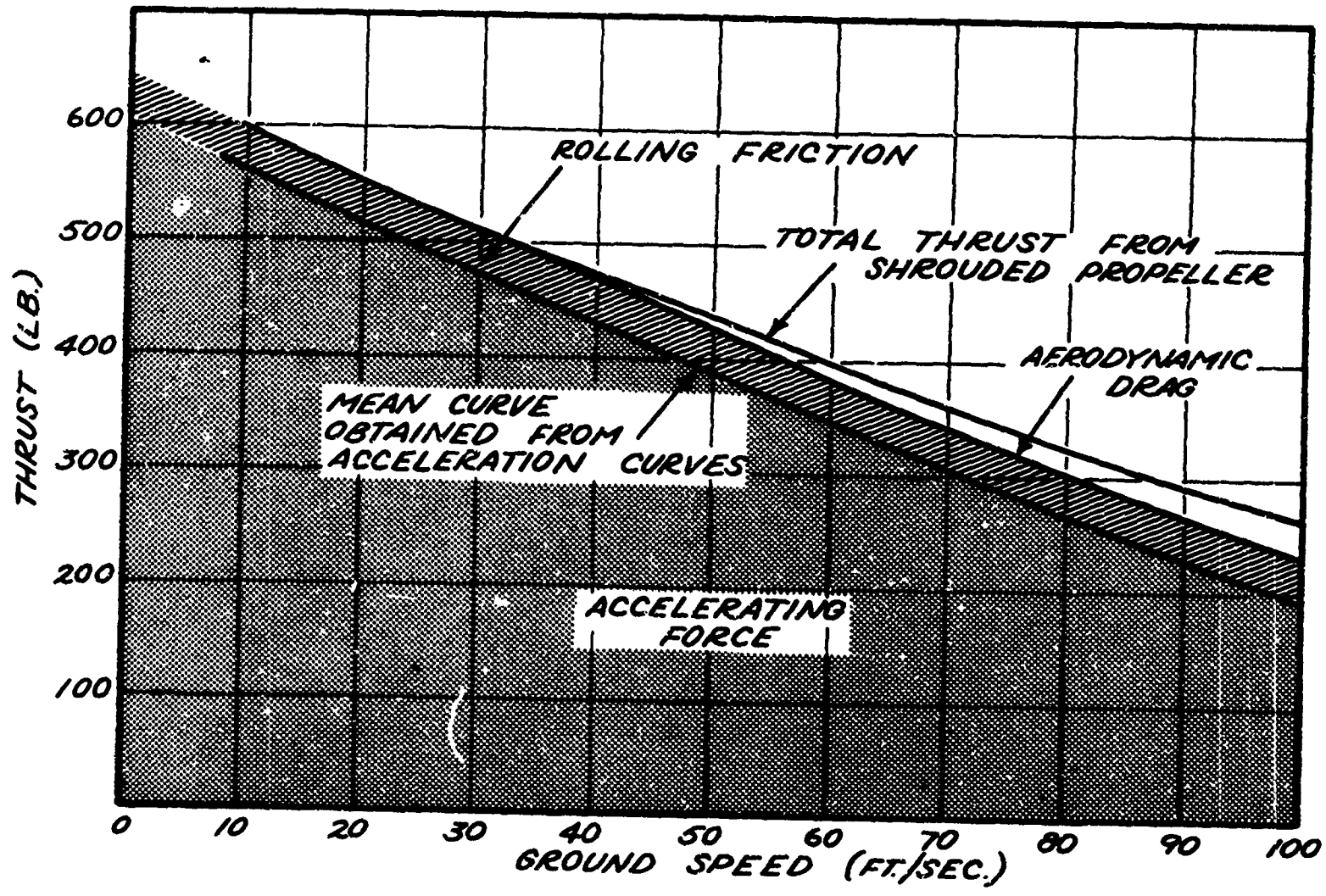

Figure 27. Shrouded Propeller Thrust Breakdown Chart From the Ground Acceleration Tests, MARVELETTE, With Twisted Propeller Blades.

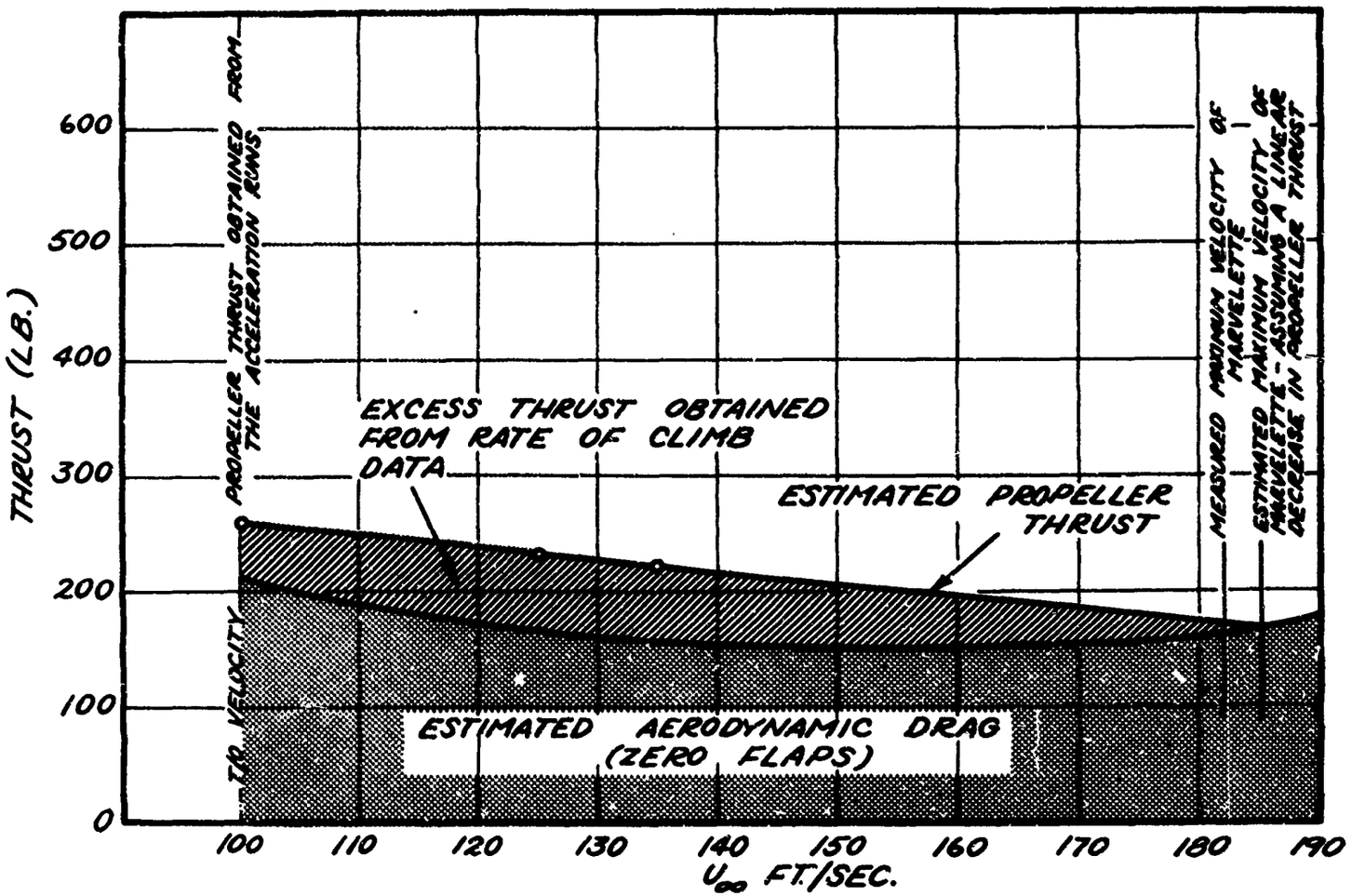

Figure 28. Extrapolation of Thrust Curves Obtained From Ground Tests to Flight Speeds.

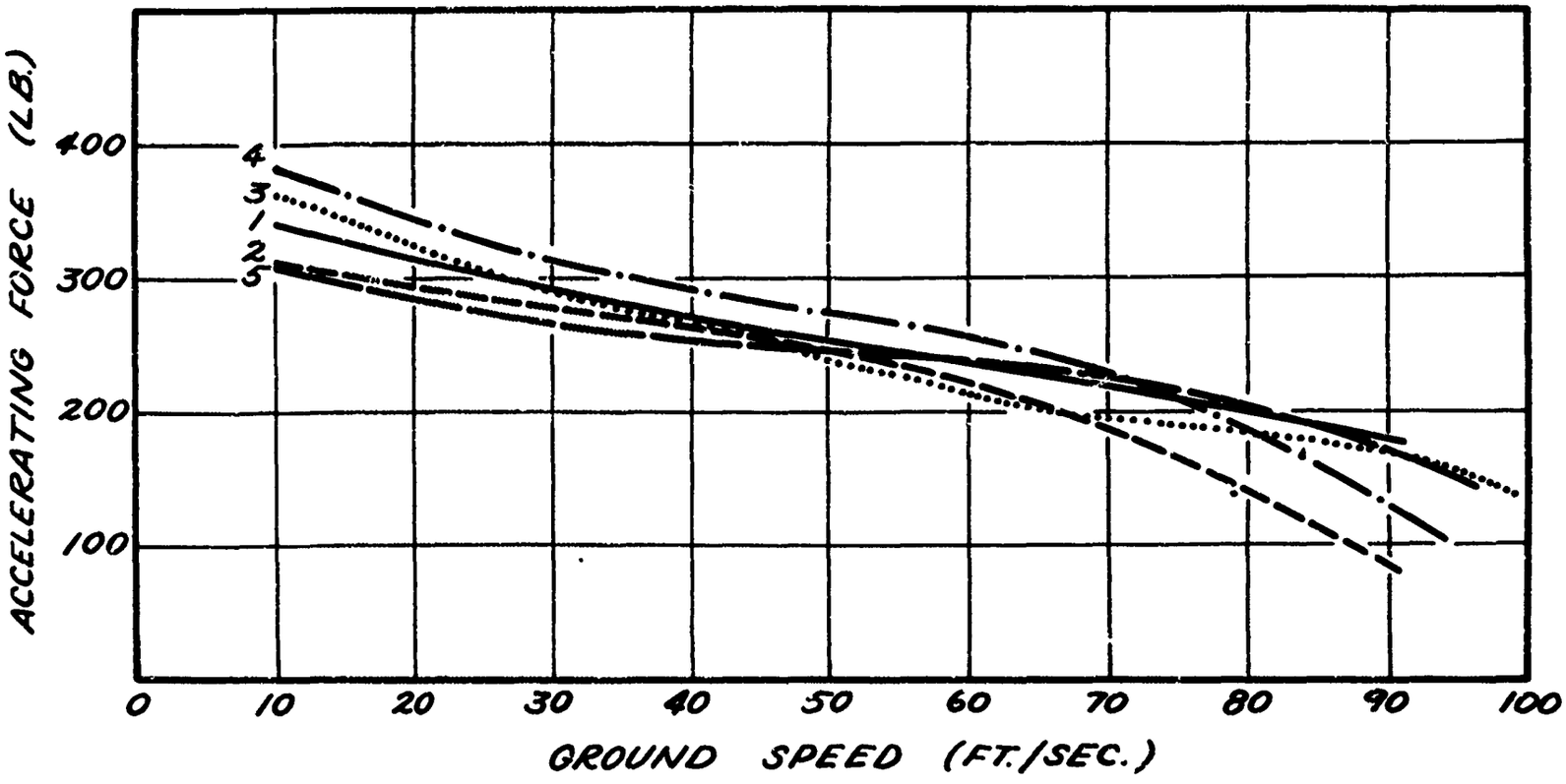

Figure 29. Curves of Thrust Available for Acceleration up to 100 Feet Per Second for the AG-14 Aircraft.

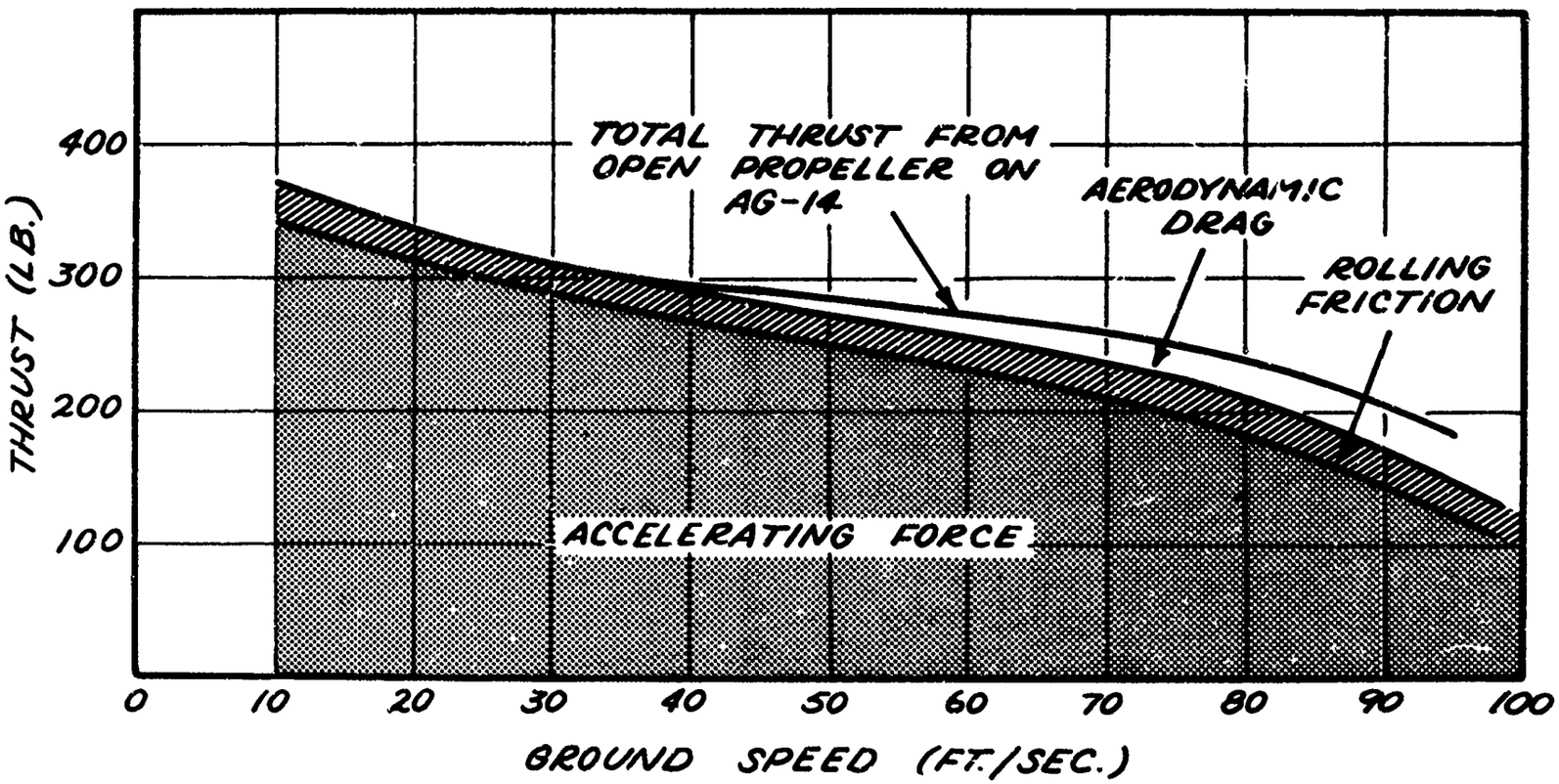

Figure 30. Open Propeller Thrust Breakdown Chart From Ground Acceleration Tests, AG-14.

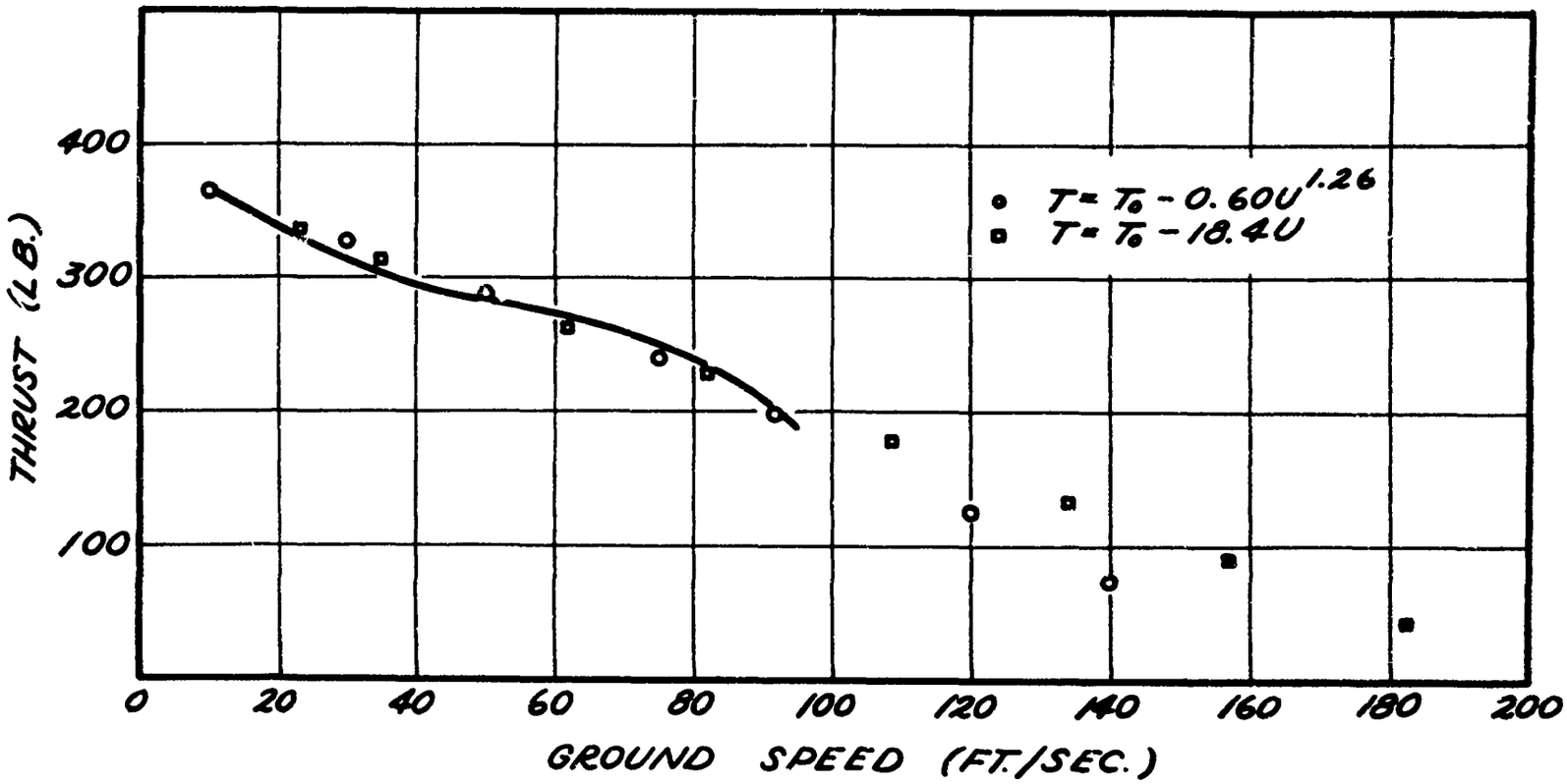

Figure 31A. Determination of an Equation for the Variation of Thrust With Forward Velocity for an Open Propeller.

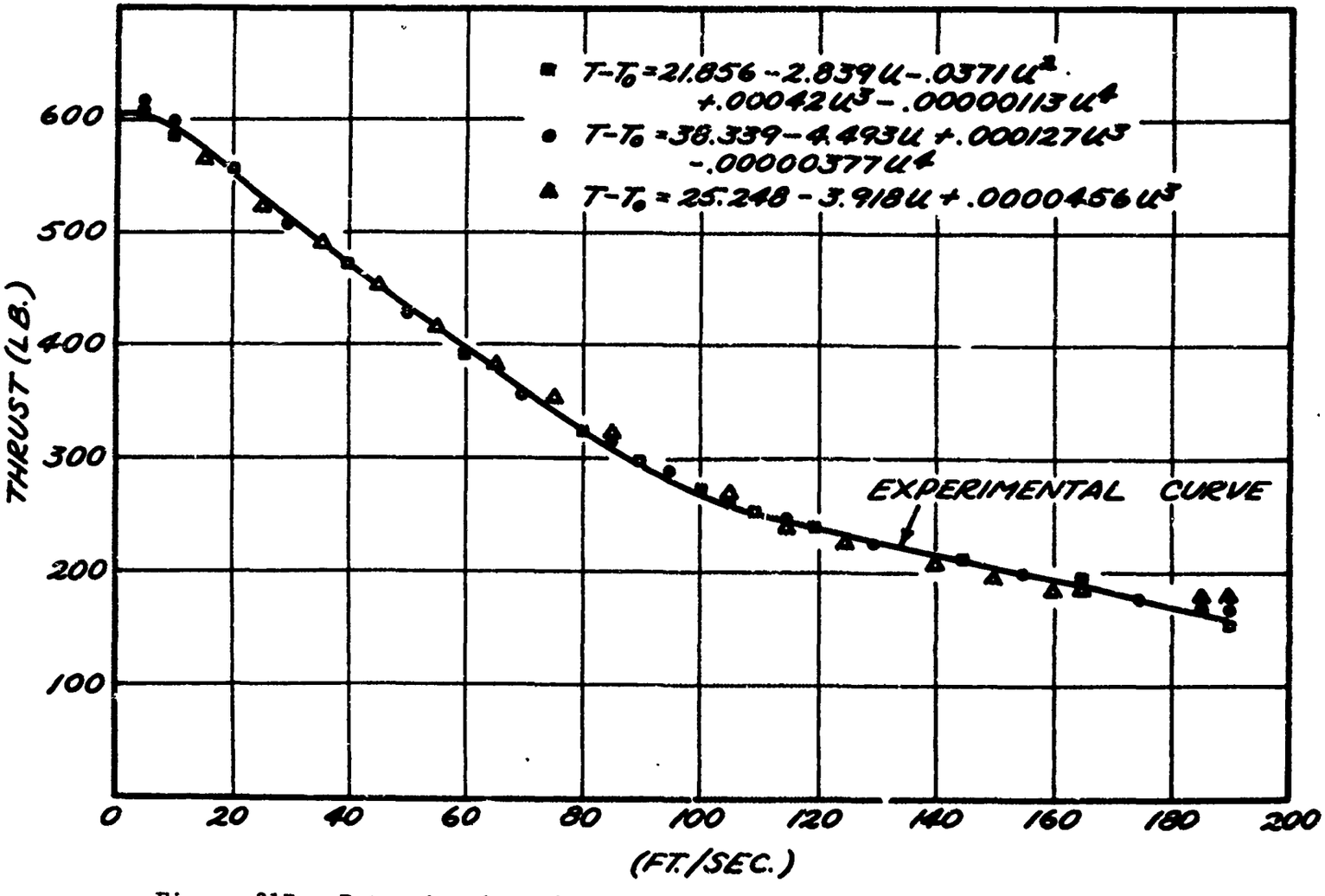

Figure 31B. Determination of an Equation for the Variation of Thrust With Forward Velocity for a Shrouded Propeller.

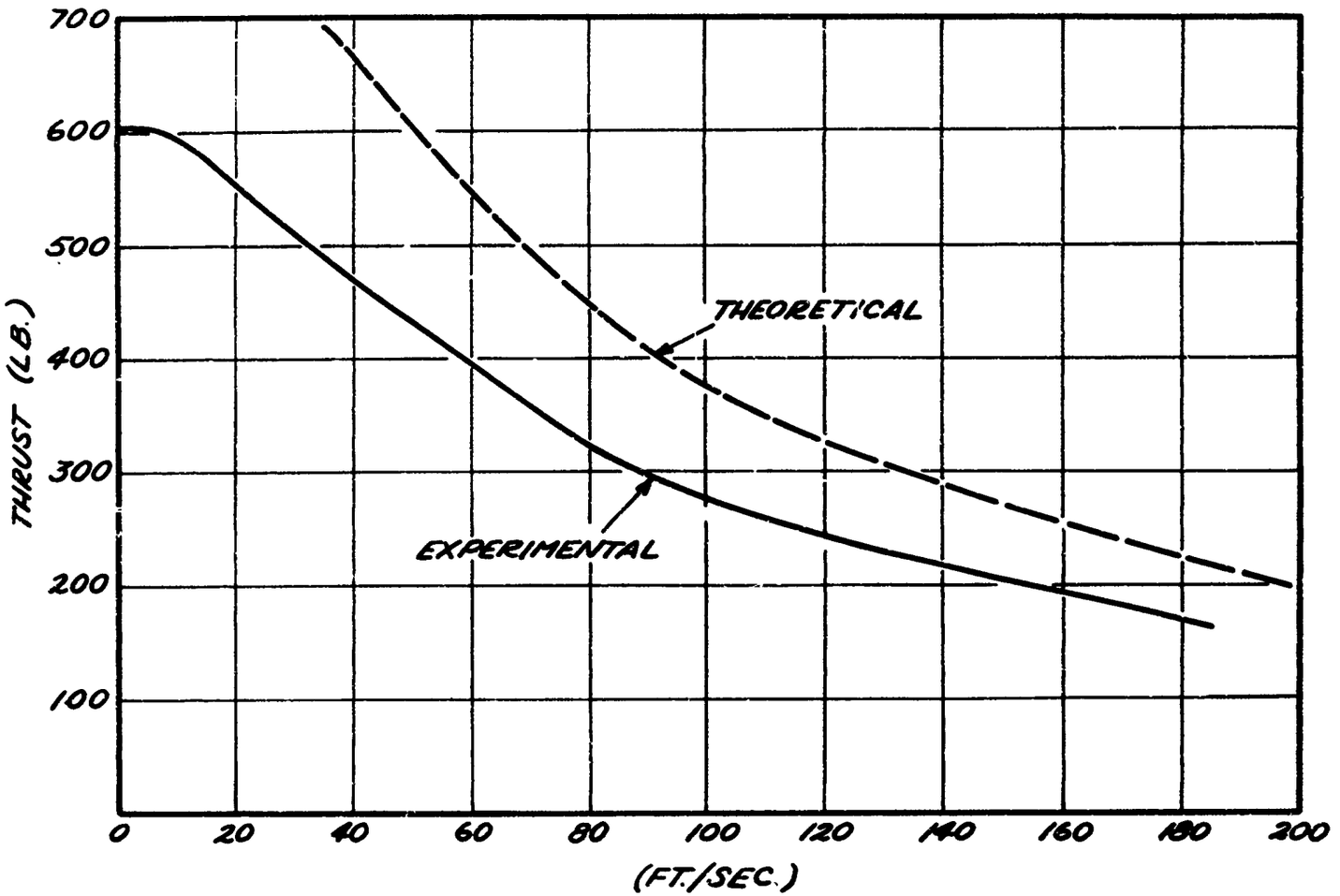

Figure 32. The Theoretical and Experimental Difference in Thrust Between a Ducted and an Open Propeller.

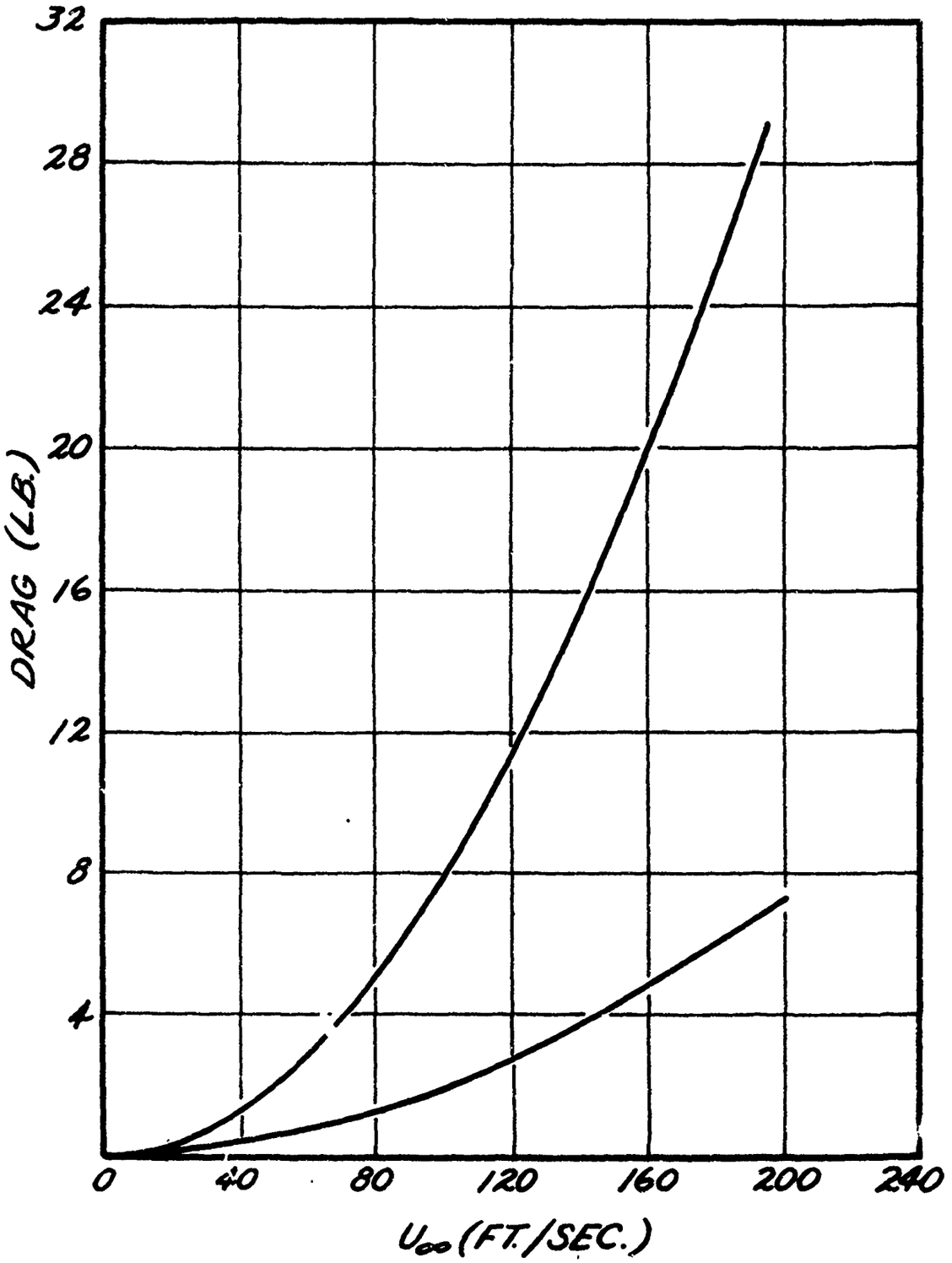

Figure 33. Estimated Drag of a Conventional and a Ring Tail Plane for the MARVELETTE Aircraft.

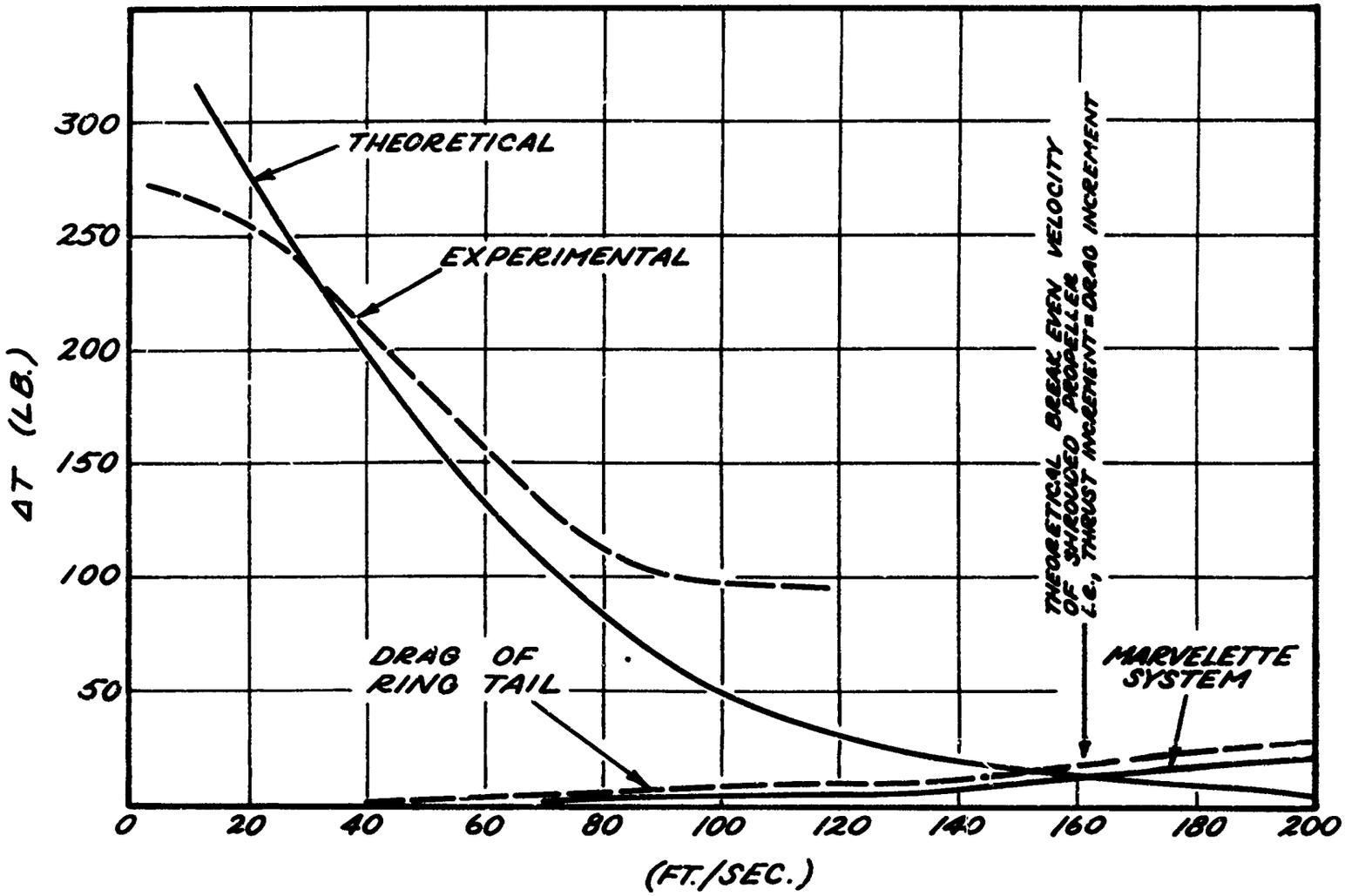

Figure 34. Comparison of the Theoretical and Experimental Variation in Thrust With Forward Velocity for the MARVELETTE Shrouded Propeller.